NATIONAL AERONAUTICS AND SPACE ADMINISTRATION

Technical Report 32-1541

Effects of Storage Temperatures on Silicon Solar Cell Contacts

Paul Berman
R. K. Yasui

JET PROPULSION LABORATORY
CALIFORNIA INSTITUTE OF TECHNOLOGY
PASADENA, CALIFORNIA

October 15, 1971

NATIONAL AERONAUTICS AND SPACE ADMINISTRATION

Technical Report 32-1541

Effects of Storage Temperatures on Silicon Solar Cell Contacts

Paul Berman
R. K. Yasui

JET PROPULSION LABORATORY
CALIFORNIA INSTITUTE OF TECHNOLOGY
PASADENA, CALIFORNIA

October 15, 1971

Prepared Under Contract No. NAS 7-100
National Aeronautics and Space Administration

Preface

The work described in this report was performed by the Guidance and Control Division of the Jet Propulsion Laboratory.

Acknowledgment

Robert Mueller and Willard Wall of JPL performed the large number of measurements discussed in this report.

Contents

Tables

Figures

Contents (contd)

Figures (contd)

Contents (contd)

Figures (contd)

Abstract

Solar cells having various contact systems and configurations were investigated to determine the effect of storage temperature and duration on cell electrical and mechanical characteristics. Cells having n diffused into p-base silicon, p diffused into n-base silicon, and p diffused into n-base lithium-containing silicon were studied. Contact systems of silver–titanium, silver–titanium with solder coating, silver–titanium with palladium, and electroless nickel were investigated. Also included in the study were submodules similar to those used in past JPL flight programs.

The results showed that electrical and mechanical degradations previously observed in high-humidity, high-temperature environment were the result of the combined environment and not due to the temperature component alone. Solder-coated silver–titanium contacts can be adversely affected by prolonged exposure to 150°C temperature soak and to −196°C liquid nitrogen exposure. The lithium-containing cells exhibited good electrical and mechanical contact stability with respect to the other cells tested at 150°C. The addition of palladium to the silver–titanium system presented no apparent advantage for the 150°C temperature soak, except in the case of relative top contact strength, where stability (but not absolute pull strength) was superior to the other cell types.

Effects of Storage Temperatures on Silicon Solar Cell Contacts

I. Introduction

The silicon solar cell is potentially an extremely reliable and long-lived device for conversion of solar energy into electrical energy. It operates at relatively low temperatures as compared with thermoelectric and thermionic devices and has no moving parts. It is therefore conceivable that a system making use of such energy converters could have an infinite lifetime. At the present time there appear to be two major factors which inhibit such an indefinite lifetime, namely (1) the sensitivity of the device to exposure to radiation and (2) the degradation of the device as a function of the environmental conditions to which it has been exposed. With respect to the latter source of degradation, the stability of the metal-to-semiconductor contacts appears to be the major concern. The effects of high-temperature, high-humidity environments on contact stability from both a mechanical and electrical viewpoint have been treated extensively in a previous JPL Technical Report (Ref. 1). In the present report the same extensive analysis has been performed as a function of storage at various temperatures without the addition of the high-humidity requirement.

II. Discussion of Experiments

The types of solar cells investigated and the ultimate test levels are shown in Table 1. Only cells fabricated by the two U. S. cell manufacturers presently supplying cells for flight programs were investigated. Both p diffused into $n(p$–$n)$ and n diffused into $p(n$–$p)$ cell configurations were investigated, as well as some preliminary lithium-containing p–n cells (for increased radiation resistance). Also included in this study were submodules fabricated from n–p and p–n cells similar to those used on the *Mariner* Mars 1969 (MM69) program and the *Mariner* Venus 67 (MV67)/*Surveyor* programs, respectively. The n–p submodule utilized 0.51-mm (20-mil) fused silica coverglass and the p–n submodules used 0.15-mm (6-mil) microsheet coverglass. Additional information and details concerning the submodule are given in the Appendix.

The majority of the cells had a nominal base resistivity of 2 ohm-cm with the exception of cell designs H-11 and H-13, n–p cells using 10 ohm-cm base material, and the lithium-doped cells which had a resistivity

Table 1. Solar cell high- and low-temperature storage[a]

Designation	Cell vendor	Cell type[b]	Base resistivity, ohm-cm	Size, cm	Contact metals	Contact type	Cover glass	Miscellaneous	Number of test samples at each exposure time	Number of control samples
1000 h storage at 150°C										
HL	HEK	*p–n*	20[b]	1 × 2	Ag–Ti–solderless	Corner dart	None	Lithium-doped	10	6
CP	CRL	*n–p*	2	2 × 2	Ag–Pd–Ti–solderless	Bar	None		10	6
H	HEK	*n–p*	2	2 × 2	Ag–Ti–solderless	Bar	None		10	6
H-17	HEK	*p–n*	2	2 × 2	Ag–Ti–solder	Corner dart	None		9	6
H-11	HEK	*n–p*	10	2 × 2	Ag–Ti–solder	Corner dart	None		10	6
H-13	HEK	*n–p*	10	2 × 2	Ag–Ti–solderless	Corner dart	None		10	6
–	HEK	*n–p*	2	2 × 2	Ag–Ti–solder	Bar	20-mil[c] fused silica	MM69 4 cell submodules	10	2
H-3	HEK	*p–n*	2	1 × 2	Elect Ni–solder	Bar	None		9	5
M	HEK	*n–p*	2	2 × 2	Ag–Ti–solder	Bar	None		10	5
CL	CRL	*p–n*	20[b]	1 × 2	Ag–Ti–solderless	Bar	None	Lithium-doped	9	5
1000 h storage at 125°C										
–	HEK	*n–p*	2	2 × 2	Ag–Ti–solder	Bar	20-mil[c] fused silica	MM69 4 cell submodules	6	2
–	HEK	*p–n*	2	1 × 2	Elect Ni–solder	Bar	6-mil[c] microsheet	MV67/ *Surveyor* 7 cell submodules	6	2
720 h storage at 80°C										
M	HEK	*n–p*	2	2 × 2	Ag–Ti–solder	Bar	None		10	5
H	HEK	*n–p*	2	2 × 2	Ag–Ti–solderless	Bar	None		10	5
1000 h storage at LN_2 (−196°C)										
HP	HEK	*n–p*	2	2 × 2	Ag–Pd–solderless	Bar	None		10	3
H	HEK	*n–p*	2	2 × 2	Ag–Ti–solderless	Bar	None		10	3
M	HEK	*n–p*	2	2 × 2	Ag–Ti–solder	Bar	None		10	3

[a]Cell thickness, 0.046 cm; cell material, silicon. HEK = Heliotek; CRL = Centralab.

[b]Base resistivity prior to lithium diffusion process.

[c]410 mμ cutoff and anti-reflectance coating.

before lithium diffusion of 20 ohm-cm. All n–p cells had dimensions of 2 × 2 cm and all p–n cells had dimensions of 1 × 2 cm except for H-17, which was 2 × 2 cm. All cells had a nominal thickness of 0.46 mm (18 mils). The four contact systems investigated here were (1) silver over titanium without solder coating (2) silver over palladium over titanium without solder coating, (3) silver over titanium with solder coating, and (4) electroless nickel with solder coating. Two basic top surface contact configurations were investigated, namely (1) a configuration using a "bar" contact extending along one edge of the cell and (2) a "corner dart" contact configuration utilizing two triangular pads, one at each of two corners of the cell, with a very narrow strip connecting the two triangles. All the contact configurations and systems have been used on flight programs with the exception of the palladium-containing systems. In all cases, except for the submodules, the sample size was 9 or 10 for each test condition. Control samples which remained unexposed to the various environments ranged from a sample size of 2 to a sample size of 6 as shown in Table 1. As can be seen, not all cell types were exposed to each of the environmental conditions, but rather emphasis was placed on the 1000-h storage at 150°C exposure, since this is expected to be the most severe environment of those studied here. While all the contact systems and configurations are of interest, those of prime interest are the palladium-containing and non-palladium-containing silver–titanium contacts without solder and the silver–titanium contacts with solder coating.

At each exposure time and temperature (indicated as data points on the respective curves) the quantities of cells indicated in the next to last column of Table 1 were removed from the test chamber, electrically measured, and pull-tested. The cells for each exposure time and temperature were systematically selected to initially represent the electrical characteristics of the unexposed groups. Electrical data was tabulated with respect to short-circuit current, open-circuit voltage, maximum power current, maximum power voltage, and maximum power for each of the exposure times and for the unexposed condition. The ratios of these values to the unexposed values were also tabulated. The average value, standard deviation, and the 95% confidence limits were determined for each of the parameters. Similarly, the contact pull strengths at each of the exposure times for each of the contact system designs were determined as were the average pull strength, the standard deviation, and the 95% confidence limits.

III. Test Facility and Procedure

A. Solar Simulation

The illumination source used throughout this test program to determine the light-generated current–voltage characteristics was a Spectrolab Model X25L close-filtered solar simulator. This simulator uses 19 lenticular lenses in the optical system that filter and uniformly distribute a relatively collimated light beam at specific distances from a 2.5-kW short-arc xenon lamp such that the resultant spectral distribution approaches that of space sunlight.

The light beam provides a 30-cm-diam (12-in.) beam pattern having a uniformity of approximately ±2% at the test plane and illumination level of 140 mW/cm^2 (one solar constant). All solar cells measured under the solar simulator were measured at 140 mW/cm^2 and test temperature of 28 ± 1°C. The solar intensity and spectral integrity of the solar simulator are constantly monitored and maintained in conjunction with the NASA/JPL Solar Cell Standardization Program.

B. Contact Strength Test Facility and Procedure

Special contact strength test tabs were standardized for this test program. Tin-plated photo-etched kovar (iron, nickel, and cobalt alloy), 0.1-mm-thick tabs were selected for use in evaluation of the subject cells. Each test tab is prebent in a forming fixture at a 90-deg angle before the cells are soldered. The soldering operation is accomplished semiautomatically by use of a Sippican Model RS-333 reflow soldering system. A solder preform (62% Sn, 36% Pb, 2% Ag) was used on all solar cells that were not solder coated. The solder joint area, assuming an additional area of about 10% for the solder fillet, was calculated to be 3.42 mm^2. To minimize electrode heating during the soldering reflow operation the soldering time–temperature profile or heat cycle was pulsed twice at a reduced voltage and pulse width to obtain consistent and uniform soldering. An applied electrode load of 3.3 kg was used, and a total elapsed time of about 4 s for each soldering operation was maintained. This soldering technique was developed to minimize the effects of soldering variations which normally exist when soldering is done with hand-soldering processes. Prior to the initiation of contact strength testing and solder attachment of the test tab, each cell is visually inspected under 10× magnification and is inspected again after each temperature exposure.

The contact strength test was done with an Instron Universal Material Test Machine Model TM-1 and a self-contained portable temperature-control chamber. A special test fixture was developed to adapt to the testing machine so that cells of varying dimension can be mounted and properly aligned perpendicular to the direction of the applied load. A copper–constantan thermocouple is mounted between the test specimen and the test fixture so that cell temperature can be monitored and maintained at ambient laboratory conditions of about 25°C throughout the test. The top and bottom contact strength of all cells were investigated, except for the top contacts having the "corner-dart" configuration (see Table 1). The contacts were pulled at a constant rate of 0.084 ± 0.008 cm/s, which corresponds to 5.04 cm/min, until complete separation occurred. The resultant contact strength was recorded on a strip chart recorder in the form of a stress–strain characteristic curve as a function of applied load to the point of separation. At this point the test specimens were reinspected to determine the interfacial characteristics that lead to the separation (e.g., solder failure, contact delamination, broken cell, defective tab, etc.).

C. Environmental Test Facility and Procedure

1. Elevated temperature storage. The high-temperature environmental tests described in this report were conducted in two separate temperature ovens. The 125 and 150°C temperature storage tests were conducted in a self-contained Missimers Model FT10-100X500 temperature oven which is capable of operating at set-point temperature from −73 to 260°C (−100 to 500°F). In order to minimize temperature gradients throughout the workspace (0.28 m^3), air is recirculated by employing the use of an internally mounted corrosion-resistant blower. A vapor-sealed shaft assembly is used to couple an externally mounted motor to the blower through the insulated wall of the test chamber in order to assure long trouble-free operation and maintain test validity. The workspace is 76 cm wide by 61 cm deep by 61 cm high and is heated by rapid-response electric air heaters mounted in such a fashion so that radiant heat energy will not be directly transmitted to the test specimens. The heaters are cycled by heavy-duty magnetic contactors. To prevent excessively high temperature, a safety thermostat is also included in the control circuit. Temperatures within the workspace are monitored and controlled by a Brown thermocouple potentiometer instrument. The system has a 30-cm-diam circular chart for recording oven temperature and a circular cam which is preshaped for programming temperature. The temperature control assembly is said to have an accuracy of ± 0.25% and sensitivity of 0.03% or better of full scale. Besides having the feature of a thermocouple break protection circuit, temperature control is provided by a time-proportional control instrument. The normal procedure used for these long-term temperature storage tests is to cycle the liquid refrigerant (CO_2) and/or hot gas, bypassing the solenoid valves, and thereby permit the compressor to run continuously to eliminate short cycling, which will result in compressor overheating due to frequent starting. Depending on set-point temperature, heat balance is provided between the radiant heat source and two cascaded mechanical refrigeration systems.

The temperature chamber used for the 80°C storage tests was a Labline Model 3505. This particular oven has a 0.1 m^3 capacity and also uses a radiant heat source (1200-W) to provide temperatures to 200°C. However, in this case an external Sim-Ply-Trol Model 4570 temperature controller and iron–constantan thermocouple are used to control a high-current (20-A) relay to regulate the input power to the oven, depending upon oven set-point temperature demand.

For handling of solar cells to and from either the Missimers or Labline ovens, a 28 × 41-cm aluminum tray lined with an 0.317-cm-thick teflon sheet was used. The test cells were laid with the sensitive surface facing upward in the tray. Power for both ovens was never reduced or turned off. The mass of the steel tray and teflon sheet caused some lag in cell temperature rise or decay rates when they were placed or removed from the temperature ovens, thereby minimizing and/or reducing thermal stresses resulting from shock.

2. Low-temperature storage. After the initial electrical performance measurements the test cells were exposed to a liquid nitrogen (−196°C) bath environment for 65 h. Subsequently the cells were removed and tested for electrical output along with the control cells and then returned to the LN_2 environment. The cells were periodically removed at 160, 285, 354, 450, 546, 642 and 1002 h total exposure at −196°C. After each interval, the cells were again measured for electrical output along with the control cells.

The −196°C environment was achieved by keeping a 17-cm-diam (ID), 3.785-liter thermos bottle filled with liquid nitrogen. To reduce evaporation rate of the liquid nitrogen, the thermos bottle was fitted with a cork stopper having a few small venting holes to prevent buildup of gas pressure. This method insured a low evaporation rate, making it necessary to replenish the

LN_2 thermos bottle only twice a week. In order to facilitate handling of the test cells when placing them into or removing them from the LN_2-filled thermos bottle, they were loaded in specially-made teflon-coated cages which restricted the motion of the individual cells and thereby eliminated the possibility of the cells striking one another. To minimize thermal shock, the cells loaded in the cages were first lowered to a position just above the surface of the LN_2 and held for about 1 min to gradually lower the temperature of the cage and test cells. The cage was then slowly submerged into the LN_2. Removal of the cage and test cells from the LN_2 was also done very slowly, and the assembly was again held at a position just above the surface of the LN_2 for about 1 min before it was completely removed.

Photographs of the test facility are presented in Figs. A-1 through A-8 in the Appendix.

IV. Data Reduction and Analysis

To aid in the analysis of the effects of different environments on the performance characteristics of various types of photovoltaic devices, a computer program has been developed to show the behavior of five important solar cell parameters as a function of exposure to the environment. This behavior is depicted in three ways; (1) a plot of the actual parameters vs time of exposure, (2) a plot of the actual parameters "normalized" to unexposed values vs time of exposure, and (3) a printed output of actual raw data.

The five solar cell parameters considered for evaluation in the program are:

Short-circuit current, I_{sc}

Open-circuit voltage, V_{oc}

Maximum power current, I_{mp}

Maximum power voltage, V_{mp}

Maximum power, P_{max}

Values for the first four parameters are input values, and the fifth parameter is calculated from $P_{max} = I_{mp} \times V_{mp}$. For a particular test, a series of cells is exposed to an environment for a given length of time.

During the test, the temperature and light intensity remain constant. At the beginning of the test, the four input parameters are measured. Thus the test provides data as a function of exposure time. These exposed cells are referred to as "test cells." To obtain an estimate of measurement accuracy and repeatibility, a series of control cells of types similar to the test cells are also measured electrically and mechanically; these control cells are not exposed to the environmental test. At the same selected points as the test cells, the four solar cell parameters of each control cell are measured. By depicting changes in the control cells values as the test program progresses, the test cell values can be corrected, thus reducing measurement-associated error. The printed output shows these values in detail.

To aid in determining statistical validity of the results of the tests, the 95% confidence limits are determined. Let X_i, $i = 1, 2, \cdots, n$ be the short-circuit current values for a series of n cells. Define the following: Let

$$Y \equiv X_1 + X_2 +, \cdots, + Xn \tag{1}$$

$$Z \equiv X_1^2 + X_2^2 +, \cdots, + X^2n \tag{2}$$

The average, 95% confidence limits, and standard deviation are given by the formulas:

$$\text{Av} = Y/n \tag{3}$$

$$\text{SD} = \left(\frac{nZ - Y^2}{n(n-1)} \right)^{1/2} \tag{4}$$

$$\text{Conf} = \frac{k \cdot \text{SD}}{\sqrt{n}} \tag{5}$$

where k is the multiplying factor which fixes the confidence limits at any desireable level. The values for Eqs. (3), (4), and (5) appear on the printed output.

To present an overall view of the test results, a set of plots is also included as part of the output. Five plots show the change of the five solar cell parameters as a function of exposure time, and five additional plots depict the normalized (to the unexposed) parameters as a function of the same variables. The plots consist of the average values, the 95% confidence limits, and a least square fit to the average using a polynomial of the second order ($Yc = a + bx + Cx^2$). If, however, data was taken at less than five points during the test program, no least square fit is plotted by the computer. The contact strength test data is treated in a similar manner.

Representative computer printout plots of the data obtained are presented as a supporting data package in Ref. 2.

A. Temperature Soak, +150°C

1. Mechanical characteristics. The relative top contact strengths of the cell types as shown in Table 1 are presented as a function of exposure time at a temperature of 150°C in Fig. 1. It can be seen that the palladium-containing contact system exhibited an increase in contact strength of approximately 15% after 1000 h exposure, while the *Mariner* Venus 67 (MV67) type cell using solder-coated electroless nickel contacts, type H-3, exhibited a decrease in top contact strength of 65%. This indicates the very great differences in stability among the cells types investigated. The lithium-containing cell, type C1, having the non-palladium-containing silver–titanium solderless system, exhibited an increase of 5%, the non-palladium-containing silver–titanium solderless and solder-coated contact systems exhibited a decrease of 20%, and the *Mariner* Mars 1969 (MM69) submodule exhibited a decrease of 35%. On an absolute basis, the *Mariner* MM69 type cell, with the solder-coated silver–titanium contact, exhibited the highest top contact strength, averaging almost 2000 grams, while the MV67 type cell, solder-coated electroless nickel, exhibited the lowest average top contact value of less than 500 g, indicating very drastic differences among the various contact systems. Neither the lithium-containing cells nor the H-11 solder-coated silver–titanium contact cells fabricated by Heliotek could be evaluated for top contact strength owing to the configuration of the contact (corner dart). The lithium-containing cells fabricated by Centralab, however, were quite low on an absolute strength basis compared with the *Mariner*-type cell, but were very similar to the H-type cell which has the same contact system, namely silver–titanium without solder coating. Apparently, for the 150°C exposure, the absolute top contact strength is relatively unaffected by the presence of lithium in the base region of the cell. Also, there was no great difference in absolute top contact strength between the palladium-containing and the non-palladium-containing solderless silver–titanium contacts. It is interesting to note that the MM69 submodules exhibited a higher absolute top contact strength than either the palladium-containing or non-palladium-containing silver–titanium contacts, even though the modules were subjected to additional stresses due to the module fabrication process and the additional thermal coefficient mismatch of the interconnectors.

The relative contact strength of the bottom contact as a function of time is presented in Fig. 2. Owing to the configuration of the MM69 submodules, they could

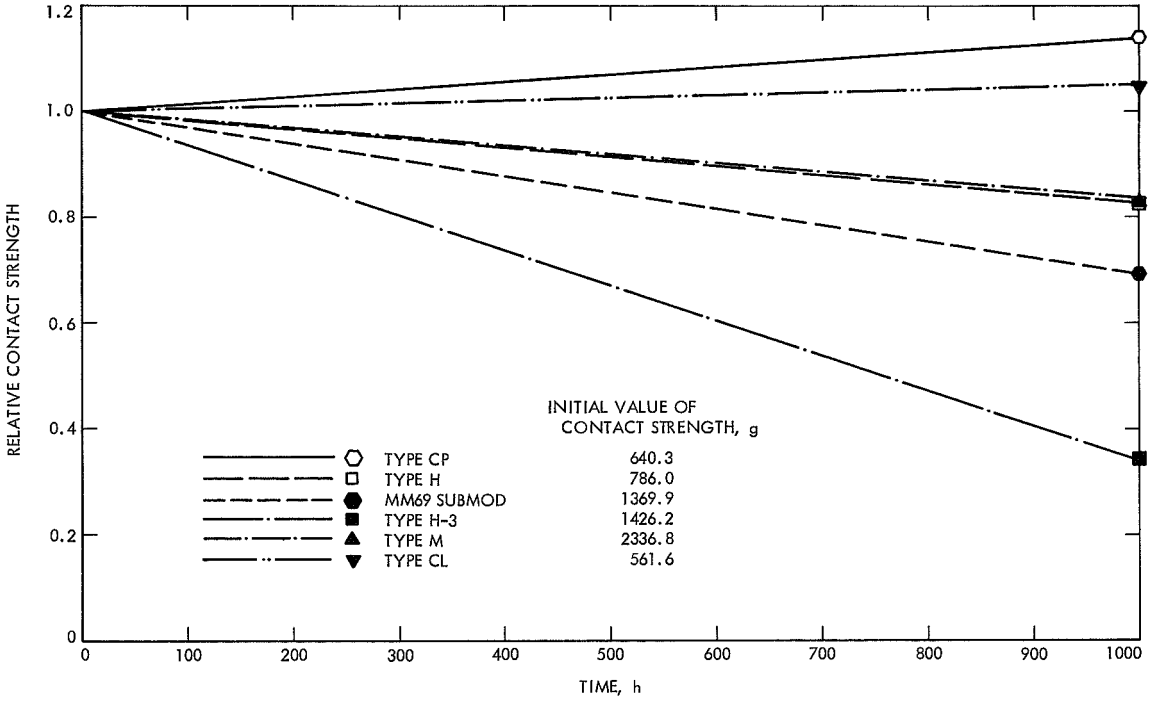

Fig. 1. Relative top contact strength of various types of silicon solar cells after long-term storage at 150°C

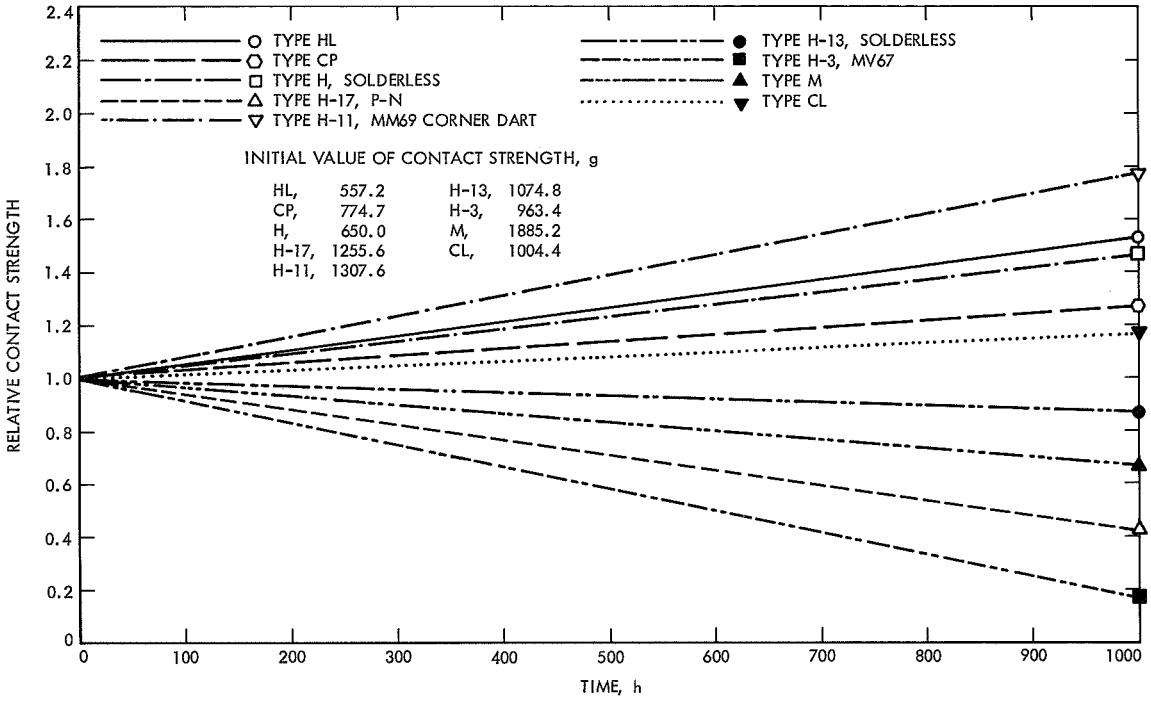

Fig. 2. Relative bottom contact strength of various types of silicon solar cells after long-term storage at 150°C

not be tested for back surface contact strength. An interesting overall pattern is observed in which five of the cell types exhibited increases in bottom contact strength while four exhibited decreases in bottom contact strength. This ranged from an 80% increase of contact strength for cell type H-11, solder-coated silver–titanium contact, to a decrease of 80% of initial contact strength for the MV67 type electroless nickel solder-coated contact system. The lithium-containing *p–n* cells with the solderless silver–titanium contact system increased by 50% after 1000 h exposure; however, on an absolute basis, the contact strength was very similar to both the palladium-containing and non-palladium-containing silver–titanium contact systems. It is of interest to note that cell type H-11, the solder-coated silver–titanium having a corner-dart configuration on the top contact, exhibited a bottom contact strength almost twice that of the MM69 type cell (type M), even though on the bottom surface the contacts were, to all intents and purposes, the same. No explanation can be made other than the possibility that the discrepancy represents batch-to-batch variations. In any case, the solder-coated silver–titanium system exhibited the highest absolute back contact pull strength.

2. Electrical characteristics. The relative short-circuit currents for the various *n–p* cell contact systems are presented in Fig. 3 as a function of exposure time. The short-circuit current parameter exhibited a high degree of stability throughout the entire test and appears to be relatively unaffected by the environment. The highest absolute short-circuit current (74 mA), based on an equivalent area of 2 cm^2, was exhibited by the corner-dart configuration of silver–titanium with solder coating (type H-11), while the other cell types all exhibited values of 66–68 mA for a 2-cm^2 area.

The relative open-circuit voltage of the *n–p* cells as a function of exposure time is shown in Fig. 4. Again, the stability of this parameter appears to be quite good for the exposure times investigated here. The solderless silver–titanium corner-dart contacts (Type H-13) actually appeared to exhibit a slight increase in open-circuit voltage during the test; however, the type H silver–titanium solderless bar contact appeared to exhibit less of an increase, so this trend may have no real significance. At most, the difference was less than ± 1%, which is within measurement accuracy.

The relative maximum power current of the *n–p* cells as a function of exposure time is shown in Fig. 5. Again, the stability of this parameter seems to be quite good for the exposure times studied, the values ranging from an increase of 2% for the solderless silver–titanium corner-dart cell to a decrease of 1% for the MM69 type cell. The

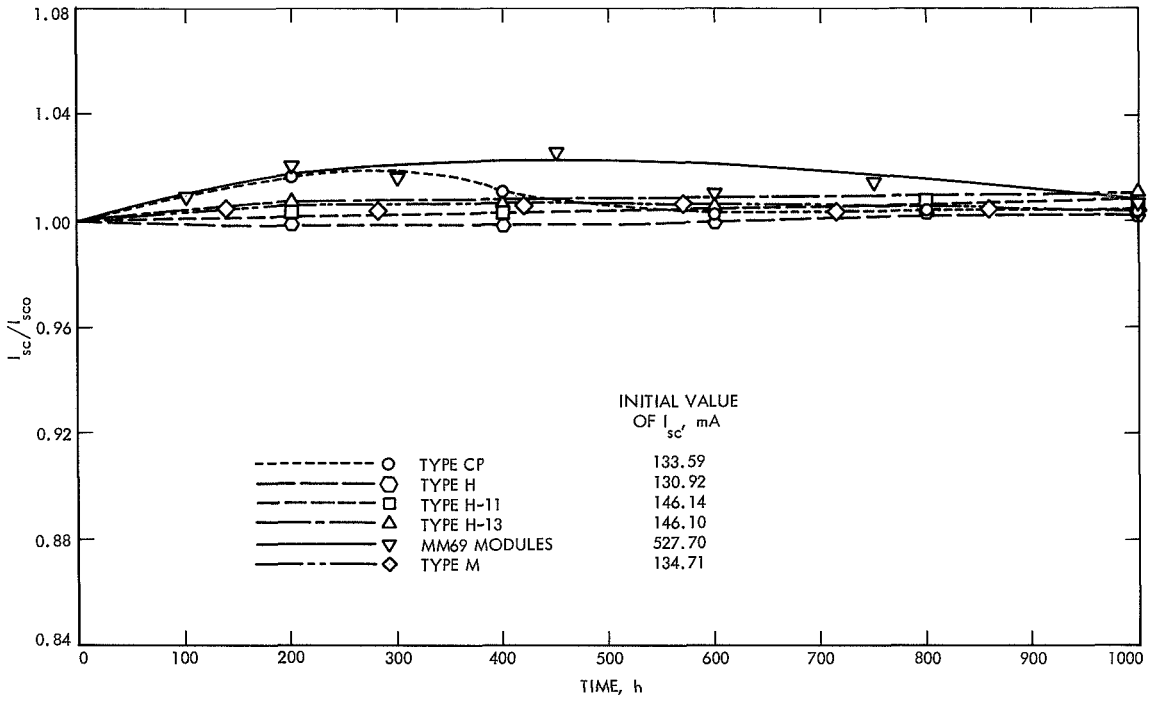

Fig. 3. Relative short-circuit current output of *n–p* silicon solar cells after long-term storage at 150°C

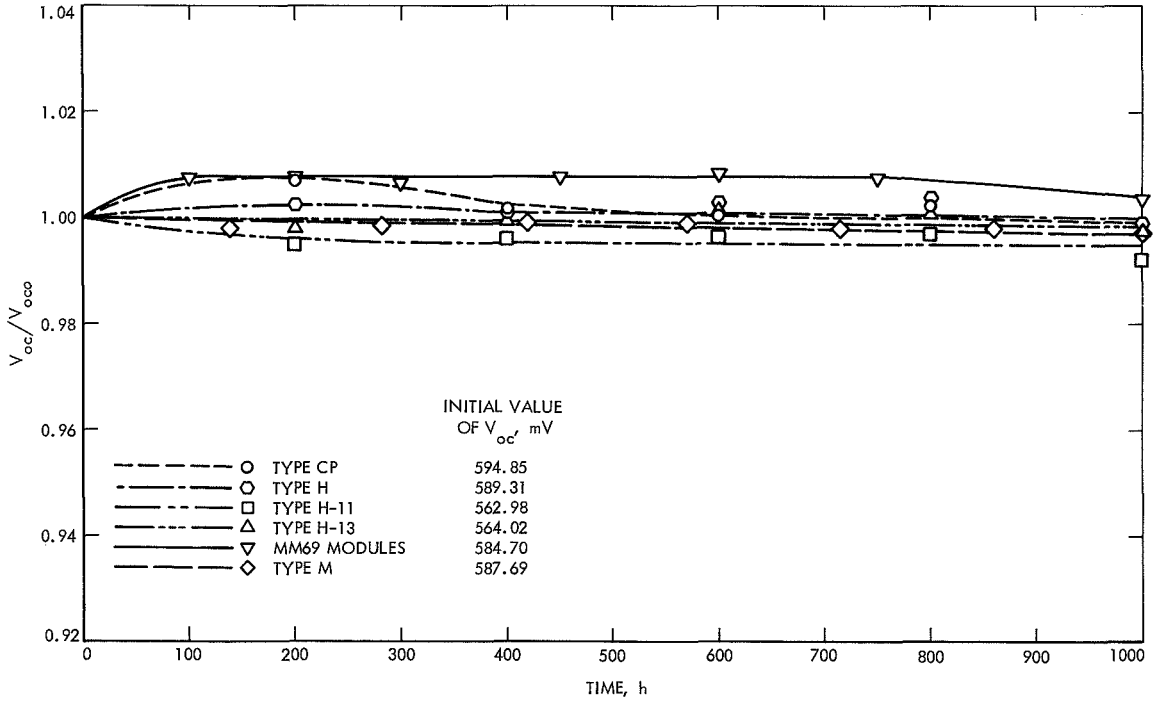

Fig. 4. Relative open-circuit voltage output of *n–p* silicon solar cells after long-term storage at 150°C

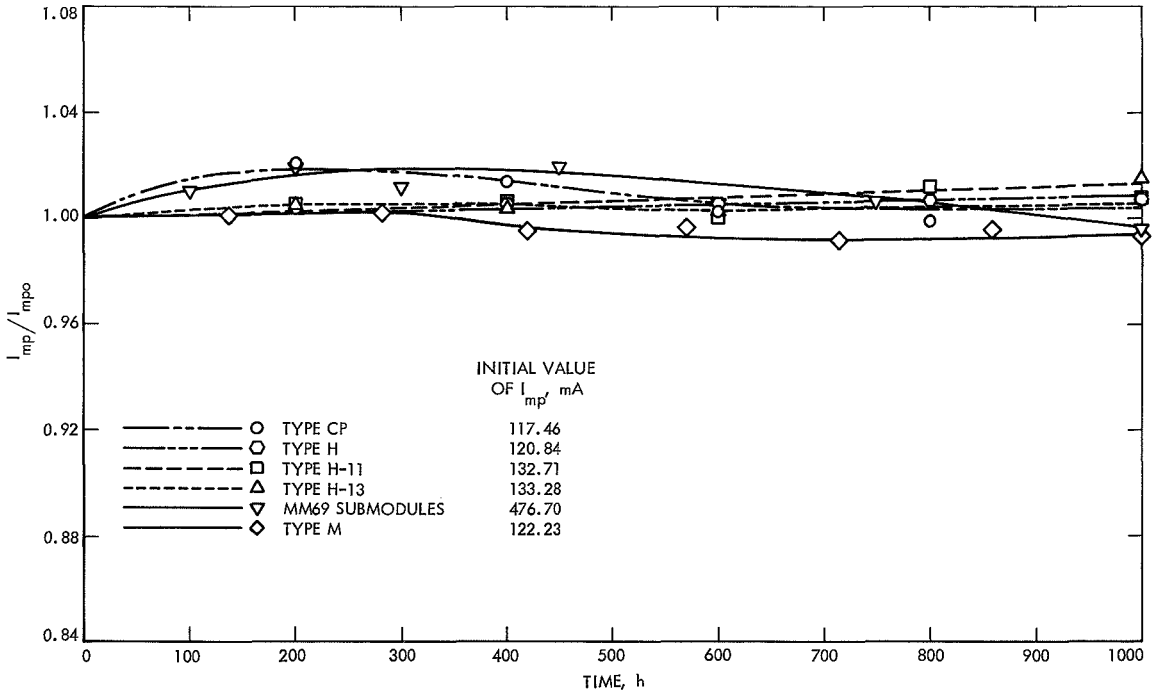

Fig. 5. Relative maximum power current output of *n–p* silicon solar cells after long-term storage at 150°C

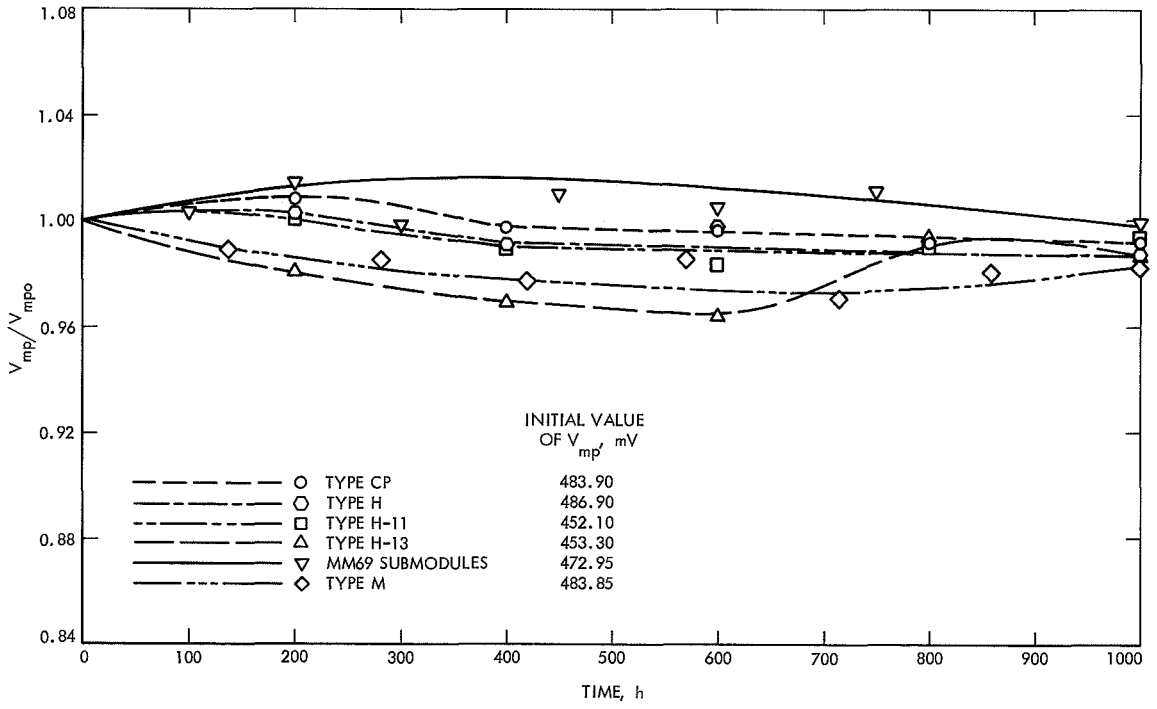

Fig. 6. Relative maximum power voltage output of *n–p* silicon solar cells after long-term storage at 150°C

relative maximum power voltage as a function of exposure time shown in Fig. 6 exhibited a wider range of stability characteristics between the cell types. The curves appear to diverge at an exposure time of about 200 to about 800 h and appear to be converging again at 1000 h. After 500 h exposure, the MM69 modules exhibited an increase of 2%, and the solderless silver–titanium corner-dart cells (H-13) were down by 3%. After 1000 h the H-13 cells and the MM69 modules exhibited no significant net change from the initial values. The absolute values after 1000 h range from 480 mV for the type H cells (silver–titanium with no solder coating) to about 500 mV for the silver–titanium solder-coated cells with a corner-dart configuration.

The relative maximum power as a function of exposure time is presented in Fig. 7. The curves appear to go through some very interesting gyrations, the significance of which is unknown, but after 1000 h all curves, with the exception of the *Mariner*-type cell, appear to converge towards a value almost identical to the unexposed value. The MM69 type cells appear to be down in power by about 2% of the initial power. The absolute values of maximum power output were also quite similar for all cell types, ranging from a power output of 28 mW for the MM69 submodules to a value of 30 mW for the silver–titanium solder-coated corner-dart cells (type H-11). (All values have been corrected to correspond to a 2-cm^2 area).

Figures analogous to those presented above for the *n–p* cell configurations were obtained for the *p–n* configurations. The decision to separate the two cell polarities was a very pragmatic one, in that had all the curves been presented together they would have been extremely confusing to the eye. The relative short-circuit current for the *p–n* cells is shown as a function of exposure time in Fig. 8. As opposed to the results of the *n–p* type cells, which indicated considerable stability of the short-circuit current parameter as a function of exposure time, the *p–n* type cells exhibit a divergence of stability depending upon contact type. The lithium-containing Heliotek cell exhibited an increase of short-circuit current of 4%; the lithium-containing Centralab cells exhibited no change; the MV67 type cell decreased by 5%; and the cells using the silver–titanium solder-coated contacts with a corner-dart configuration decreased by 13%. The lithium-containing Heliotek cells were considerably lower in initial short-circuit current (having an initial I_{sc} of approximately 58.5 mA) than the other three cell types (including the lithium-containing Centralab cells), which had short-circuit currents of approximately 66 mA based on a 2-cm^2 area. The increased short-circuit current observed in the lithium-containing cells or the lack of degradation may possibly be due to a redistribution of the lithium atoms within the base of the cell as the result of exposure to the temperature, and may therefore be the result of contact effects plus lithium redistribution effects. The decrease of about 5% observed for the MV67 type cells is in line with past experience with this type of contact (electroless nickel, solder-coated). The rather drastic decrease of 14% of the solder-coated silver–titanium contacts is unexpected but is probably attributable to the unfamiliarity of the vendor with the deposition of this type of contact on this type of cell. These cells were made on a laboratory basis since all previous experience with *p–n* cells (other than the lithium-doped cells) has been with the electroless nickel, solder-coated contact on a 1 × 2-cm cell.

Cells similar to the *p–n* H-17 type (silver–titanium contacts on a 2 × 2-cm cell) were also purchased without solder coating to compare the effects of solder coating on the cell characteristics. Upon inspection, however, it was discovered that these cells were so deformed ("bowed") that accurate electrical measurements could not be performed, and therefore they were rejected for inclusion in this study. The H-17 cells with solder coating were usable because the solder configuration compensated for the deformity. It is, however, reasonable to expect that the stresses which caused the deformation of the cells without solder coating would still be operative (perhaps even enhanced) in the solder-coated cells. Thus, these built-in stresses, believed to be at least partially a result of the *p–n* junction diffusion operation (particularly severe for the larger 2 × 2-cm cell size) might have been instrumental in causing the large degradations observed in these tests.

The relative open-circuit voltage of the *p–n* cells is shown as a function of exposure time in Fig. 9. This parameter appears to be quite stable for all *p–n* cell types except for the solder-coated silver–titanium contacts (H-17), which exhibited a degradation of about 5%. Again, this is most likely due to the fact that these cells were fabricated on a laboratory basis.

The relative maximum power current as a function of exposure time for the *p–n* cells is shown in Fig. 10. The stability of the maximum current parameter can be seen to vary considerably depending on cell contact type, the lithium-containing Heliotek cells increasing by 5% after 1000 h and the silver–titanium corner-dart contact cells decreasing by 12% at 1000 h. The divergences have the

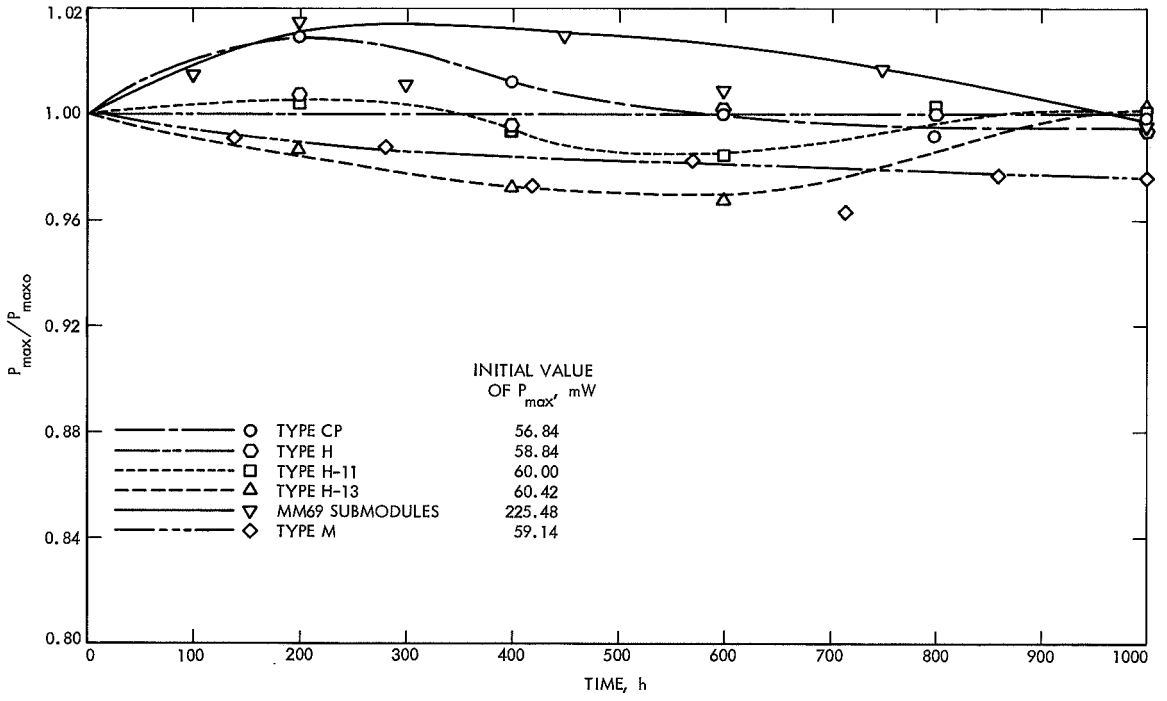

Fig. 7. Relative maximum power output of *n–p* silicon solar cells after long-term storage at 150°C

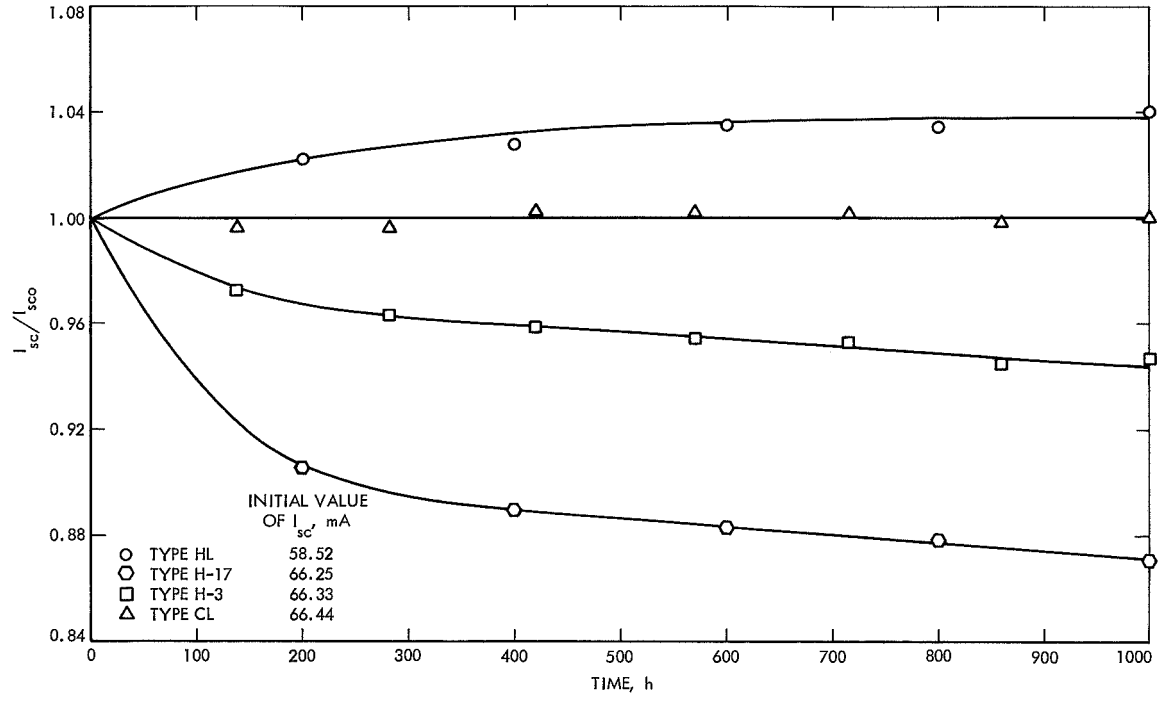

Fig. 8. Relative short-circuit current output of *p–n* silicon solar cells after long-term storage at 150°C

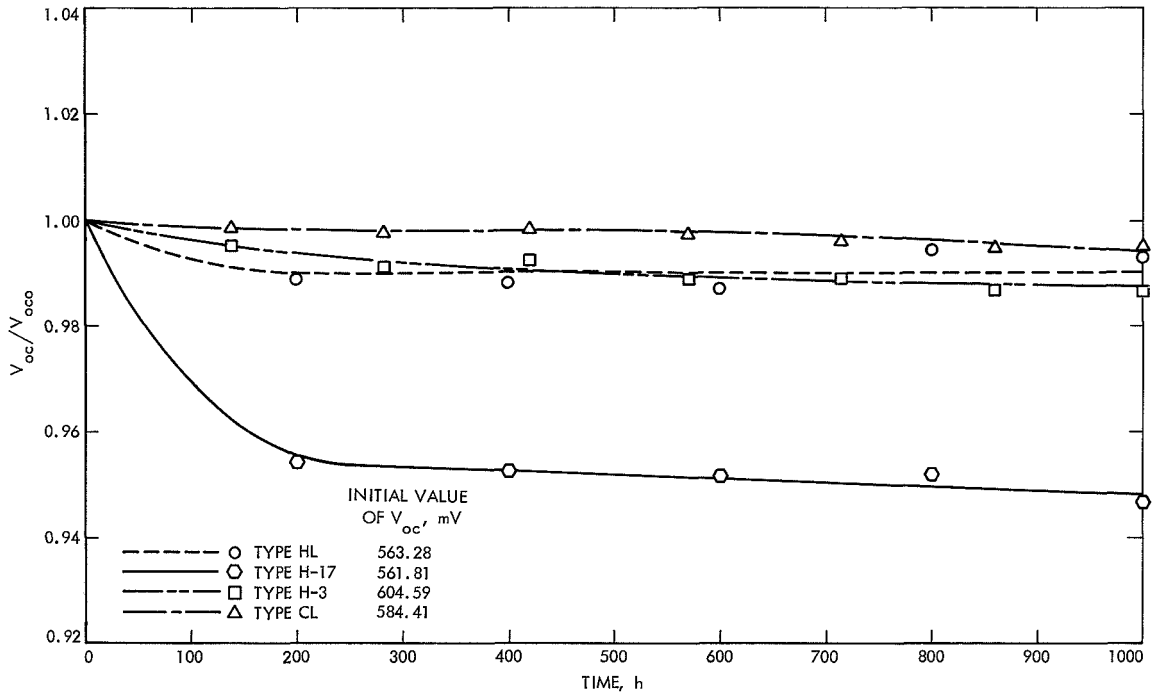

Fig. 9. Relative open-circuit voltage output of *p–n* silicon solar cells after long-term storage at 150°C

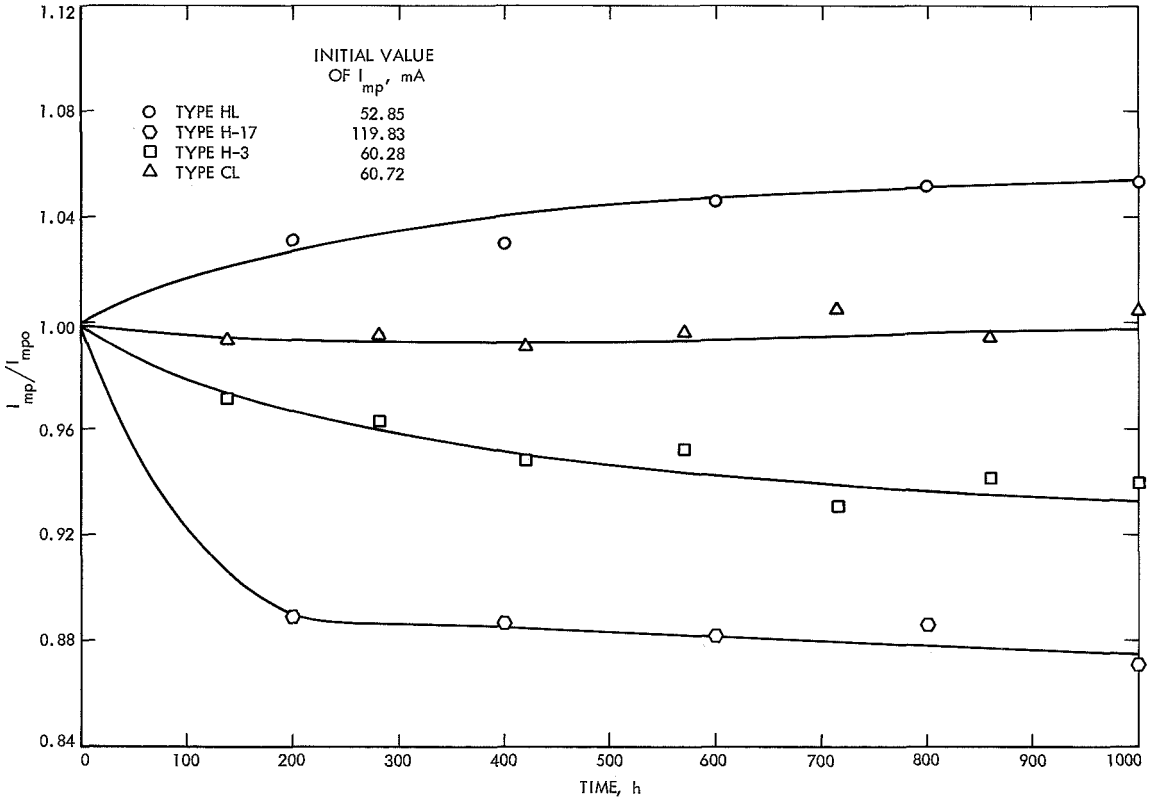

Fig. 10. Relative maximum power current output of *p–n* silicon solar cells after long-term storage at 150°C

same form as that seen in Fig. 8, which depicted the relative short-circuit current output as a function of time of exposure, and the same explanation applies here. The relative maximum power voltage as a function of exposure time is shown in Fig. 11. The lithium-containing cells, types H-L and C-L, exhibited little change as a result of a 1000-h exposure, while the MV67 type and the solderless silver–titanium corner-dart type exhibited a decrease of 6 to 7%.

The relative maximum power of the *p–n* cells as a function of exposure time is presented in Fig. 12 and shows the same general trend as seen in Fig. 8 (showing the relative short-circuit current as a function of exposure time). The lithium-containing Heliotek cells showed an increase of 7%, while the lithium-containing Centralab cells exhibited essentially no change. The MV67 type cells exhibited a maximum power degradation of 12% and the solder-coated silver–titanium corner-dart cells exhibited a maximum power decrease of 18%. Similar conclusions can be drawn for the maximum power parameter as for the short-circuit current parameter, namely, (1) the contacts of the lithium-containing cells are either more stable than the non-lithium-containing cell contacts, or the lithium in the body of the cell is interacting in such a manner as to negate any degradations occurring in the contacts, and (2) the solder-coated silver–titanium corner-dart cell degradation might be partly a result of the laboratory processing of this nonstandard configuration. The degradation might also be partly due to the interaction of the tin component of the solder with the silver component of the solder; however, the solder-coated *n–p* type H-11 cells exhibited no power loss and solder-coated *n–p* type M cells exhibited a power loss of approximately 2%. Thus the 18% power loss of the *p–n* type H-14 cell is significantly greater in magnitude, indicating additional degradation mechanisms.

B. Temperature Soak, +125°C

1. Mechanical characteristics. Relative top contact strengths of silicon solar cell submodules are shown as a function of exposure time at 125°C in Fig. 13. (Due to the contact configuration, only the top contacts could be tested for pull strength.) As shown in Table 1, the test articles were solar cell submodules fabricated from *n–p* and *p–n* solar cells and having a configuration identical to submodules used on MM69 and MV67/*Surveyor* flight programs, respectively. It can be seen from Fig. 13 that both module configurations suffered considerable top contact strength degradation as a result of this exposure; however, the MV67 configuration, utilizing cells with solder-coated electroless nickel contacts, suffered a very major degradation of greater than 50% loss in contact strength as opposed to the MM69 modules, utilizing cells with solder-coated silver–titanium contacts, which suffered a degradation of about 23%. The severe degradation of the MM67 module configuration was expected on the basis of previous tests conducted during the flight programs (thus this configuration was not included in the more severe 150°C temperature soak discussed above). Interestingly enough, the value of contact strength for unexposed submodules indicated that the MV67 modules actually exhibited a 30% greater contact strength than the MM69 submodules. Details of submodule construction differences and additional tests previously performed on submodules are given in the Appendix. It should further be noted that the contact strength degradation of the MM69 submodules was of the same magnitude in the case of the 125°C soak as for the theoretically more stringent 150°C soak shown in Fig. 1. That is to say, the degradation of contact strength of these modules was no more severe at the 150°C temperature than it was at the 125°C temperature.

2. Electrical characteristics. The relative short-circuit current of the submodules as a function of exposure time is shown in Fig. 14. The short-circuit current appeared to rapidly increase by about 1% and remained constant throughout the life of the test for the MM69 submodule configuration, while the MV67 submodules appeared to smoothly decrease to about 2% at the end of 1000 h exposure. On an absolute basis, the short-circuit current density of the MM69 submodules was about 8% higher than that of the MV67 submodules.

The relative maximum power current as a function of exposure time for the submodules is shown in Fig. 15. Again, the MM69 submodules appear to be quite stable over the length of this test. The MV67 submodules, however, exhibited a degradation of greater than 6%. The relative open-circuit voltage as a function of exposure time for the submodules varied by less than ± 1% (Fig. 16). The open-circuit voltage of both submodule types appears to be quite stable over the test time considered. The relative maximum power voltage for the submodules as a function of exposure time is shown in Fig. 17. In this case, the MM69 submodules exhibited an increase of approximately 2%, while the MV67 submodules exhibited a decrease of approximately 3%.

The relative maximum power of the submodules as a function of exposure time is presented in Fig. 18. The MM69 submodules exhibited an initial increase in maximum power of about 3% after about a 200-h exposure,

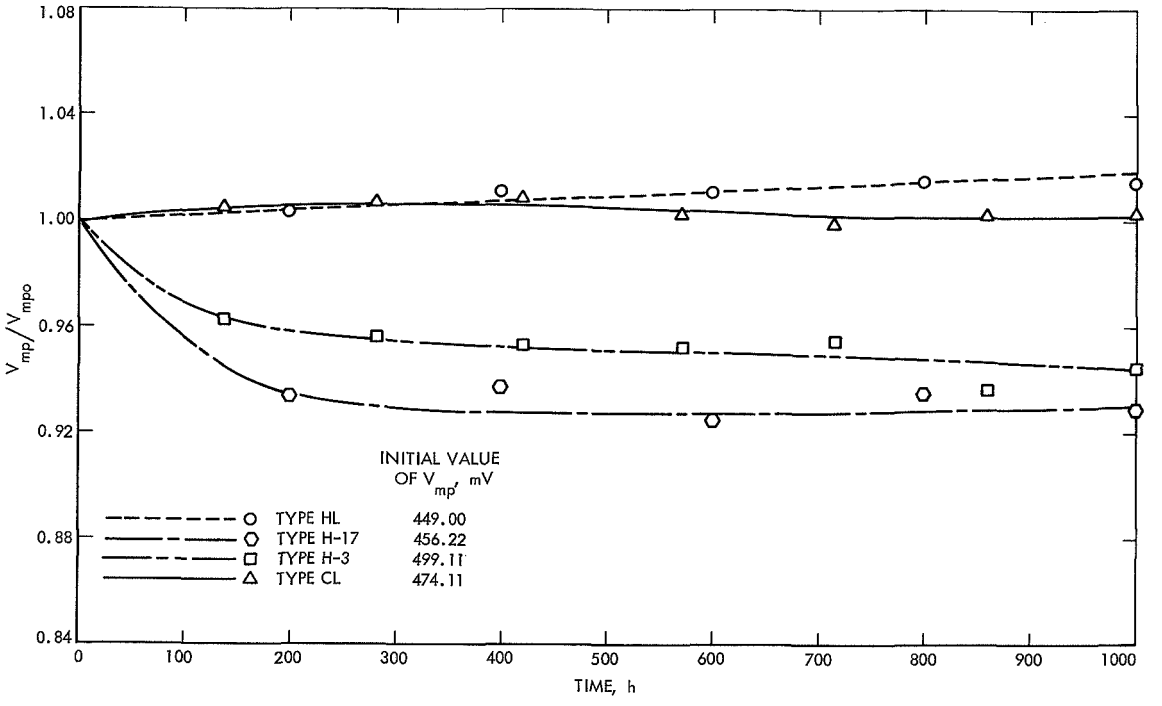

Fig. 11. Relative maximum power voltage output of *p–n* silicon solar cells after long-term storage at 150°C

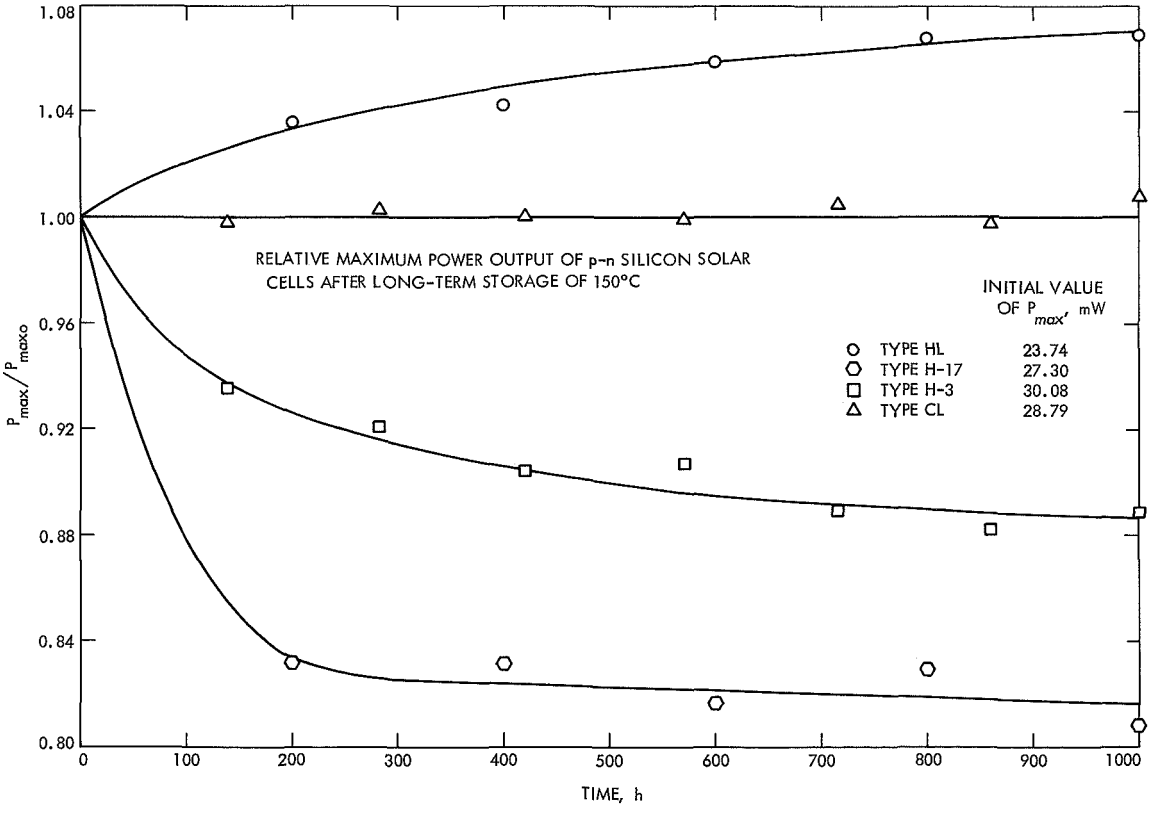

Fig. 12. Relative maximum power output of *p–n* silicon solar cells after long-term storage at 150°C

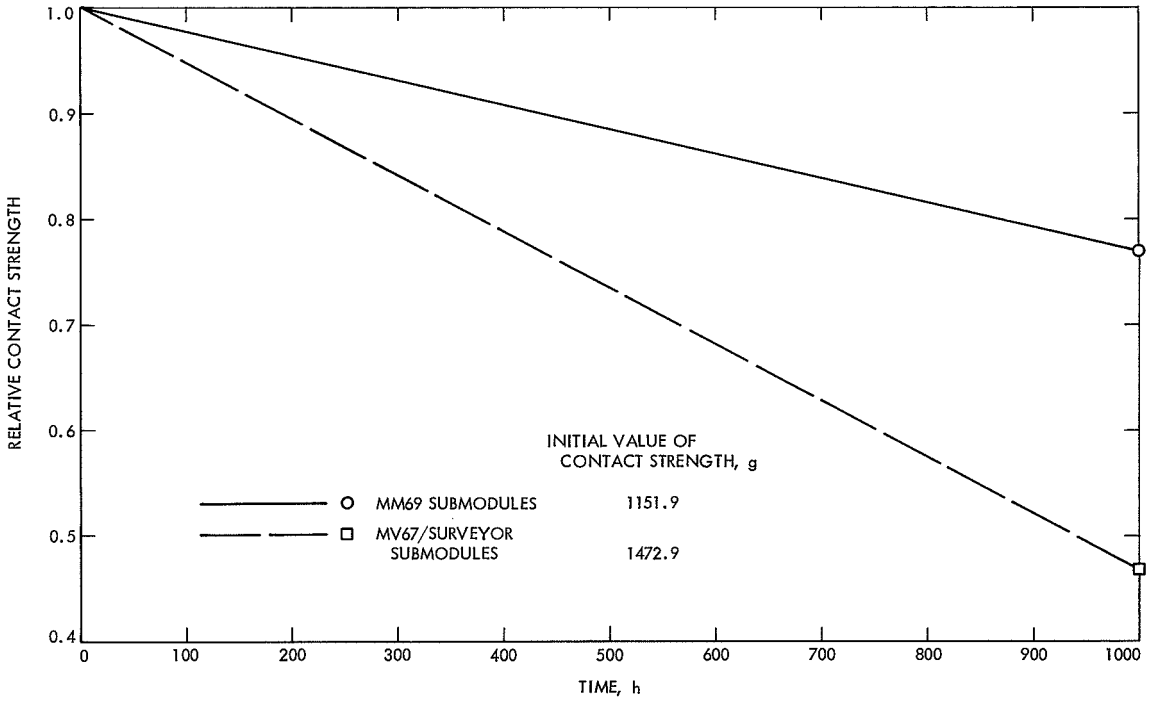

Fig. 13. Relative top contact strength of silicon solar cell submodules after 1000 hours of exposure at 125°C

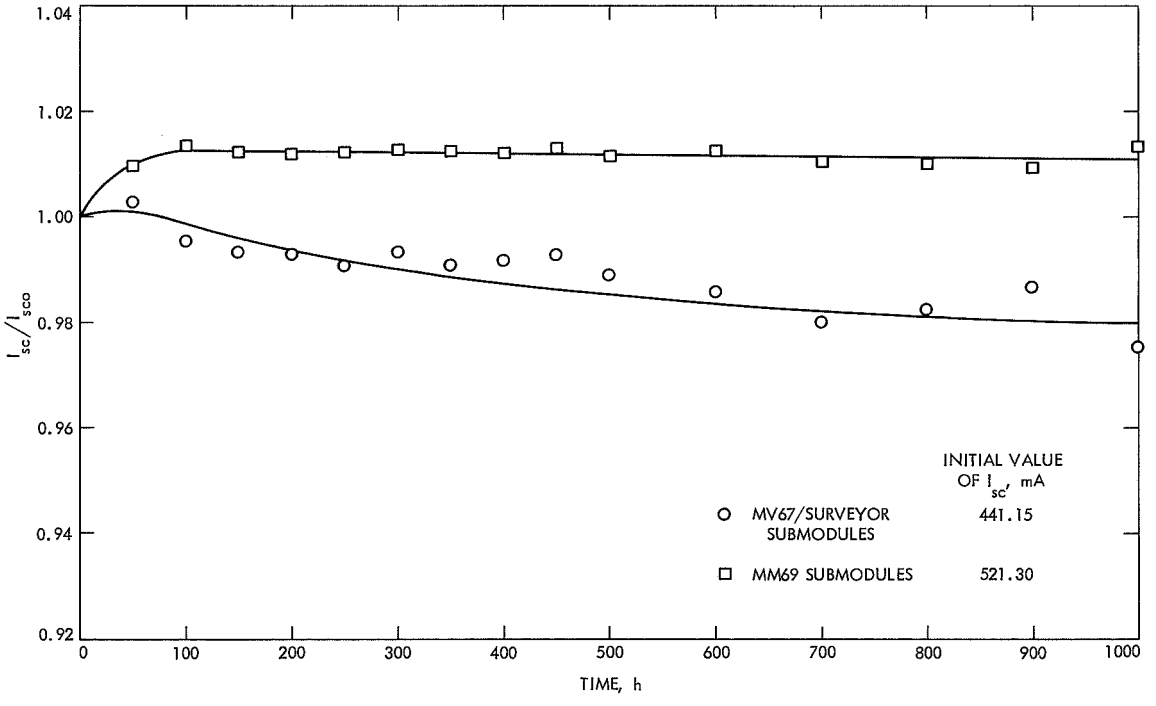

Fig. 14. Relative short-circuit current output of silicon solar cell submodules after long-term storage at 125°C

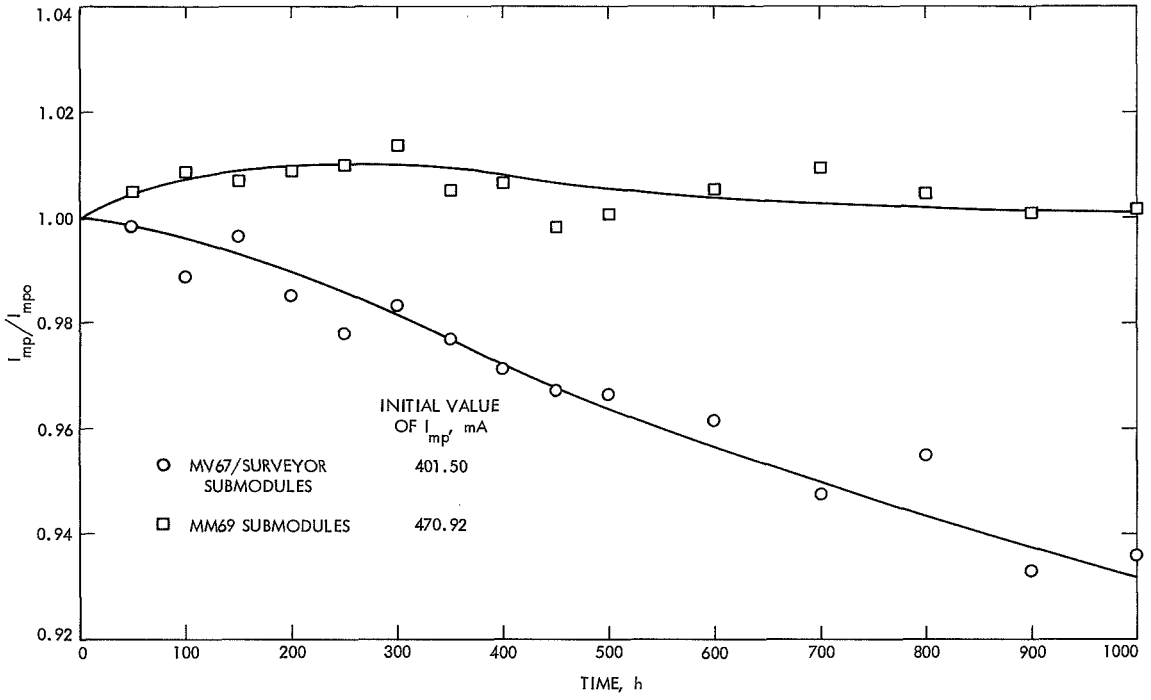

Fig. 15. Relative maximum power current output of silicon solar cell submodules after long-term storage at 125°C

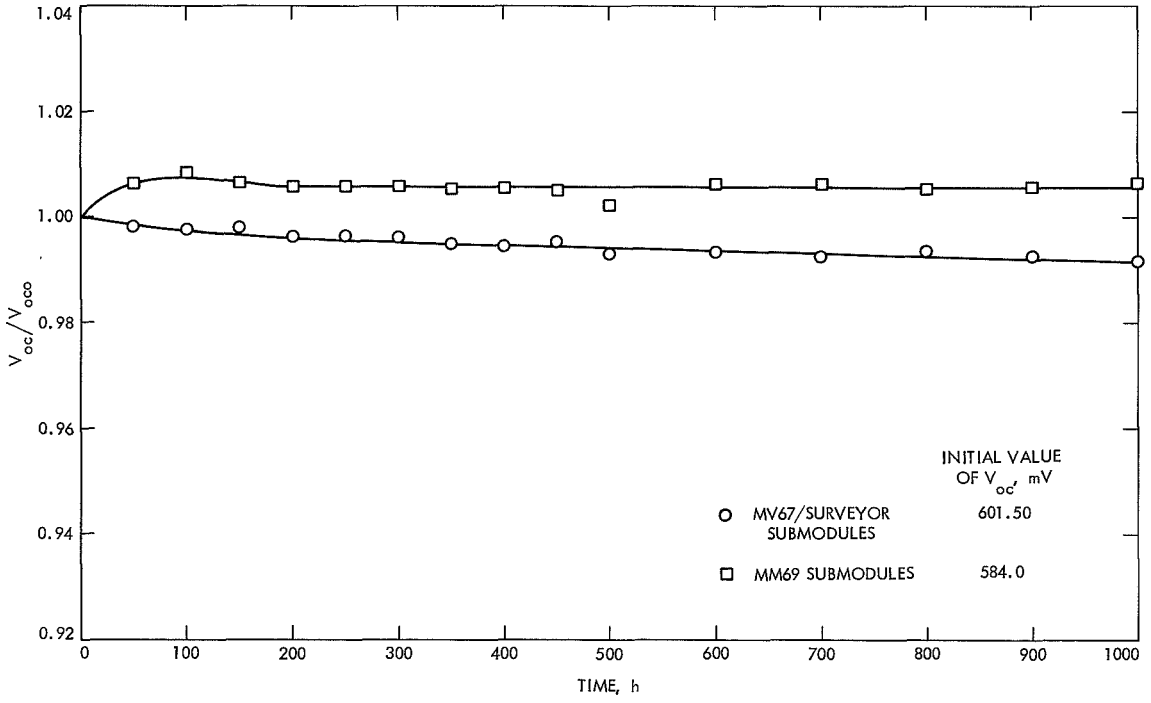

Fig. 16. Relative open-circuit voltage output of silicon solar cell submodules after long-term storage at 125°C

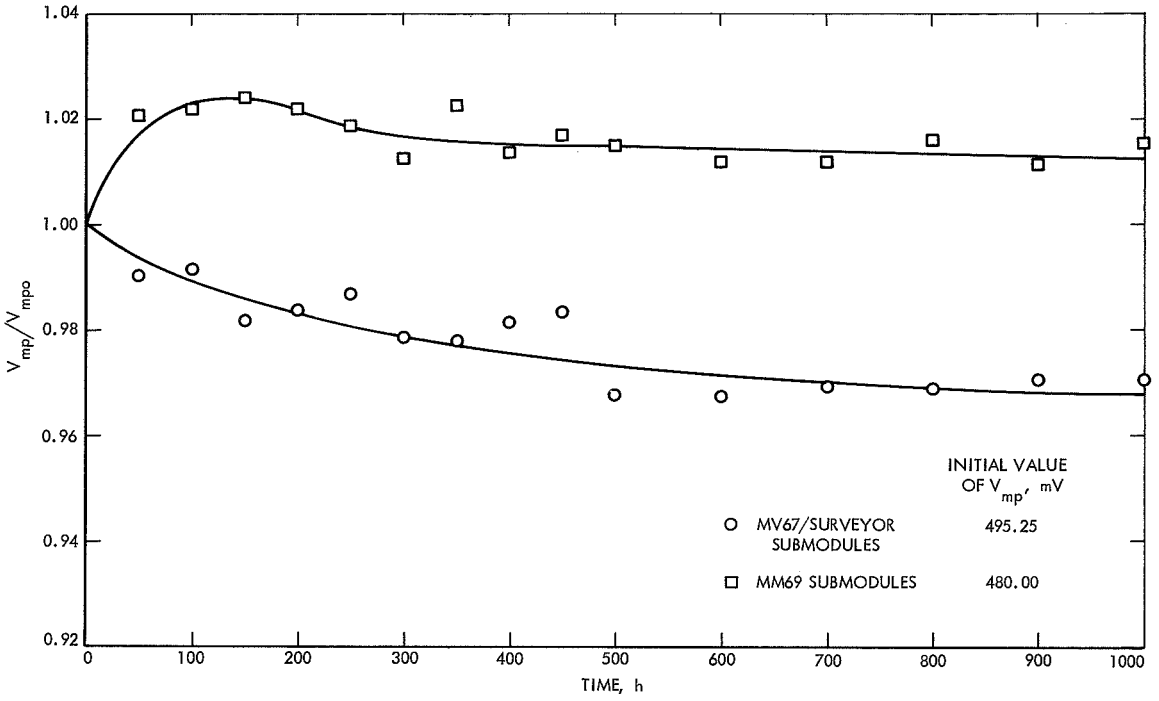

Fig. 17. Relative maximum power voltage output of *p–n* silicon solar cell submodules after long-term storage at 125°C

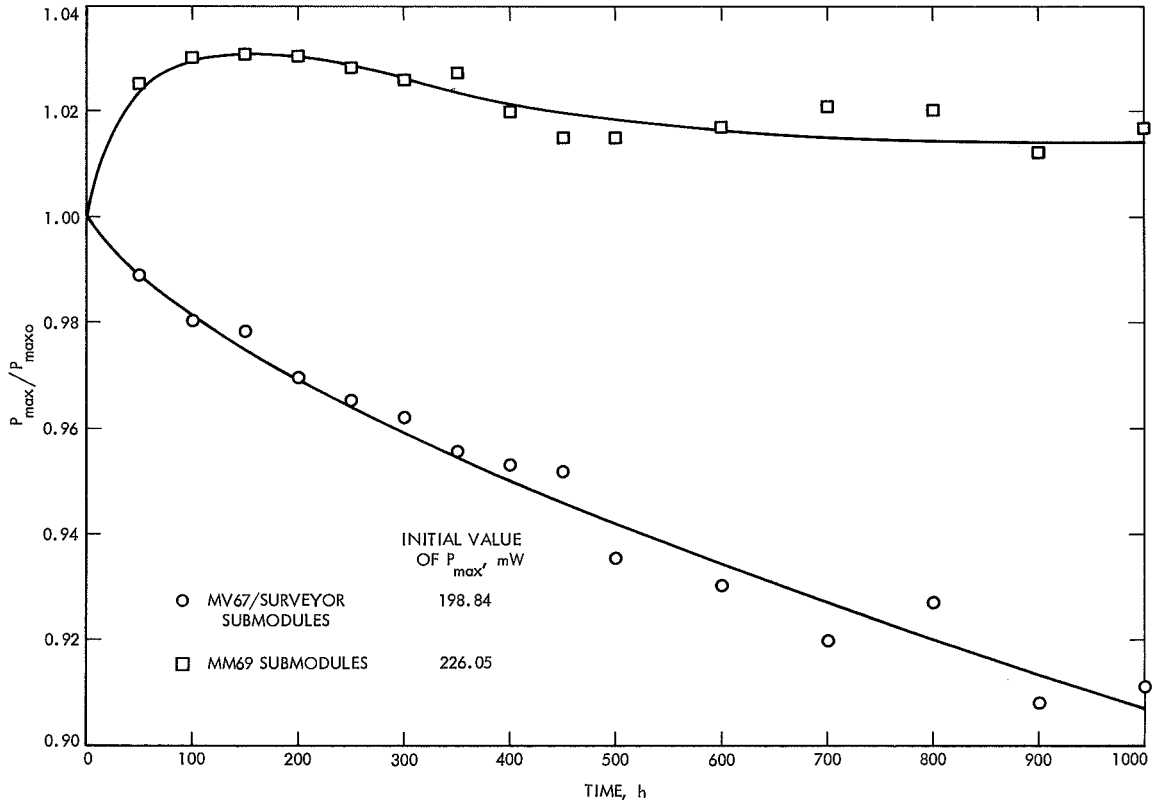

Fig. 18. Relative maximum power output of silicon solar cell submodules after long-term storage at 125°C

which was slightly reduced to a net increase of 2% after 1000 h. In contrast, the MV67 submodules exhibited a rather smooth but drastic decrease in maximum power output, reaching approximately 9% degradation after 1000 h. It can therefore be concluded that both mechanical and electrical stability of the *Mariner* 1969 submodules are considerably greater than that of the MV67 submodules and that a very significant increase in reliability has been achieved.

C. Temperature Soak, +80°C

This test, which should be significantly less severe than storage at 150°C, was performed to provide correlation with studies previously reported on the effects of a high-temperature, high-humidity environment exposure test (Ref. 1). In the latter test, the cells had been exposed to an environment of 95% relative humidity at a temperature of 80°C and a cumulative exposure time as high as 720 hours. In the high-temperature/humidity test, very significant and severe loss of contact strength had been observed for the silver–titanium contact cells without solder coating. Also, very significant electrical power loss had been observed for the silver–titanium non-solder-coated contact cells (type H). Since the type M (silver–titanium with solder coating) and type H (silver–titanium without solder coating) *n–p* cells are most commonly used for flight programs, these cells were investigated at the 80°C temperature soak.

1. Mechanical characteristics. The relative top contact strength of the two cell types as a function of exposure time is shown in Fig. 19. It can be seen that the contact strength for both cell types is quite stable over the entire soak time of 720 h. This is in decided contrast to the results previously obtained with the combined temperature/humidity environment, where the type H cells had suffered a contact strength degradation of 53%, and also in contrast to the loss of almost 20% in contact strength for both type H and type M cells which occurred after 1000 h exposure to 150°C temperature soak, as shown in Fig. 1.

The relative bottom contact strength of the two cell types is shown as a function of exposure time in Fig. 20. An even greater contrast is found in the bottom contact strength behavior as a function of exposure time, since in this case the contact strength actually increased by about 10%, whereas in the high-humidity, high-temperature environment the contact strength of the M type cells decreased by 34% and the contact strength of the H type cells decreased by 66%. Thus it appears quite clear that the severe mechanical and electrical degradations previously observed (Ref. 1) in the high-temperature, high-

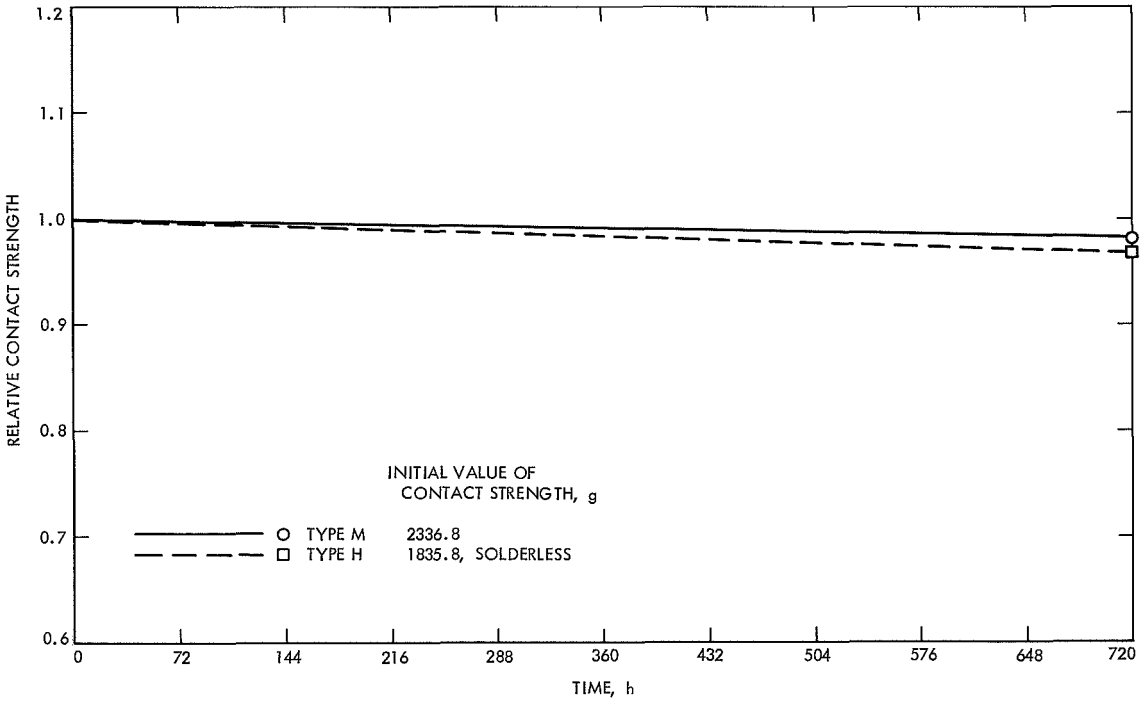

Fig. 19. Relative top contact strength of silicon solar cells after 720 hours of exposure at 80°C

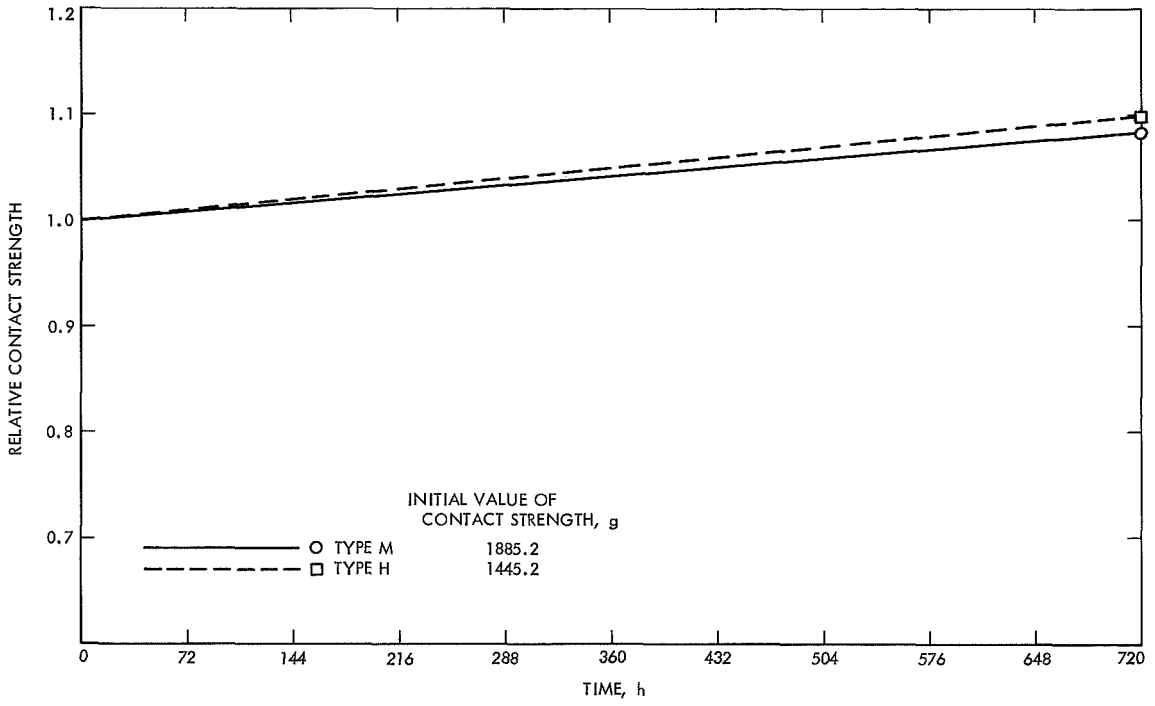

Fig. 20. Relative bottom contact strength of silicon solar cells after 720 hours of exposure at 80°C

humidity environment were the result of the combined environment rather than only the temperature aspect of the environment. For exposure at 80°C, there appears to be little difference in behavior between the type M and type H cells, whereas when the 95% relative humidity was superimposed on this temperature, a decided superiority of the type M cells was observed. After exposure to the 150°C storage temperature, as shown in Fig. 2, the type H cell exhibited a contact strength increase of about 30% after 720 h, while the type M cell exhibited a decrease of about 20%. Thus, while at the lower temperatures (80°C) there is little difference between cell types H and M in the absence of humidity, at the higher temperature (150°C), the type H cell exhibited a decided superiority in back contact strength. This is probably due to the detrimental effects of the interaction between the solder coating (particularly the tin component) and the silver–titanium contact itself at the elevated temperatures. It should be noted, however, that at the 150°C temperature, cell type H-11, solder-coated silver–titanium contacts with "corner dart" top contact configuration, exhibited a back contact strength *increase* of almost 80% as shown in Fig. 2. The reasons for the very great differences in back contact strength between solder-coated cell types M and H-11 are not known, but the results obtained on the H-11 cells indicate that the presence of solder does not *necessarily* result in mechanical degradation of the cells.

2. Electrical characteristics. The relative short-circuit current output of the two cell types as a function of exposure time is shown in Fig. 21. This parameter appears to be quite stable over the exposure time investigated, in contrast to the severe decrease in short-circuit current observed in the high-humidity, high-temperature tests performed previously (Ref. 1). In the latter tests, it had been found that a severe degradation of the silicon monoxide coating was promoted in the humidity/temperature environment. No such degradation is observed as a result of testing at the 80°C temperature alone.

The relative maximum power current as a function of exposure time is shown in Fig. 22. Again, this parameter seems quite stable over the exposure times tested. Similarly, the relative open-circuit voltage as a function of exposure time as shown in Fig. 23 exhibited very stable behavior over the exposure time tested. In the humidity/temperature environment the type H cell open-circuit voltage had been found to degrade approximately 2%. The relative maximum power voltage as a function of exposure time is shown in Fig. 24 and indicates an increase of about 2% for the type M cell.

The relative maximum power output for the two cell types as a function of exposure time is shown in Fig. 25. The type M cell exhibits a slight power increase of about 1.5% after 720 h, and the type H cell exhibits a power

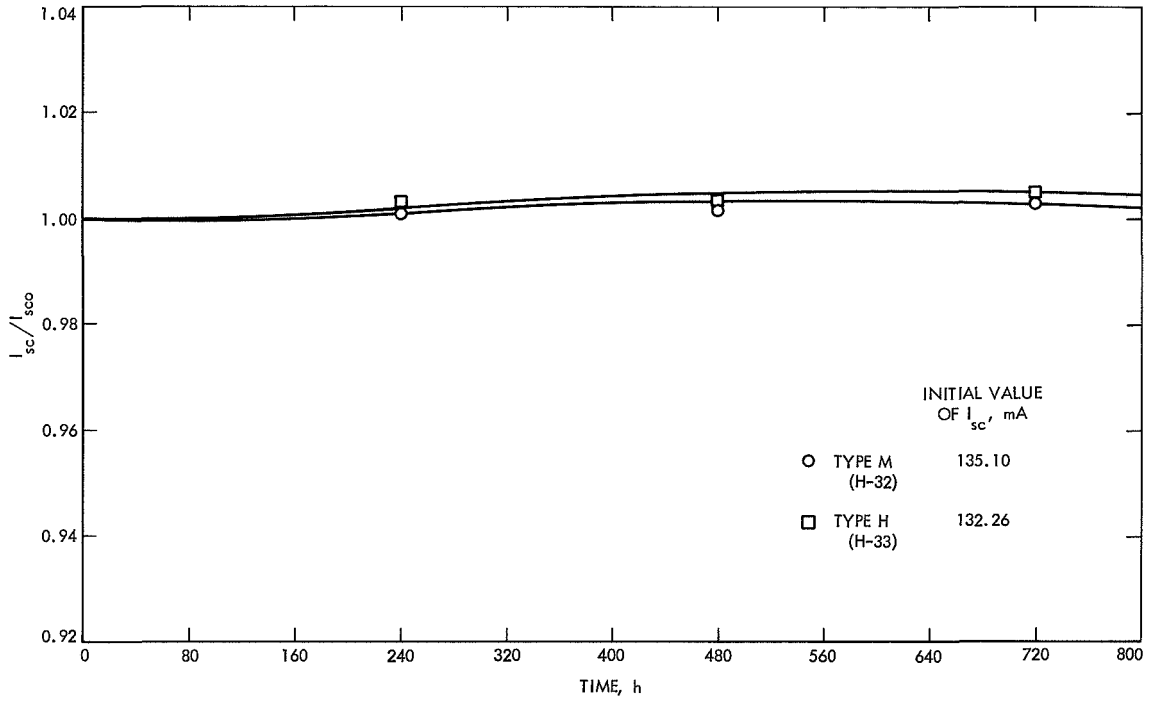

Fig. 21. Relative short-circuit current output of silicon solar cells after 720 hours of exposure at 80°C

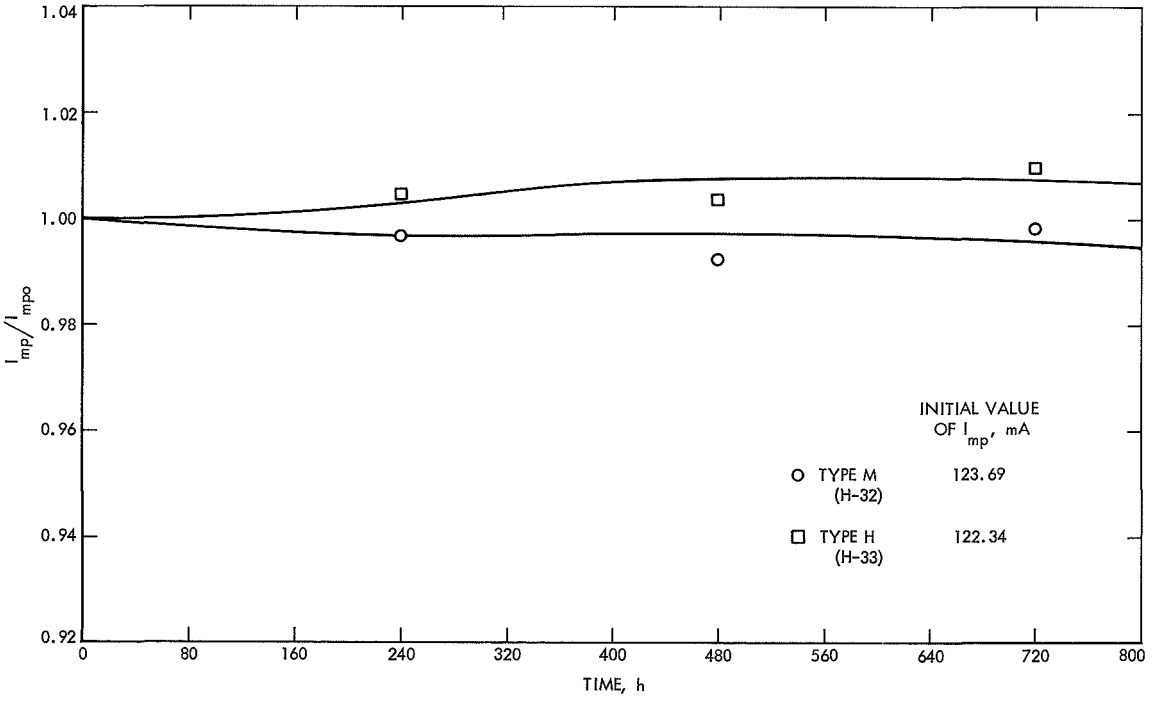

Fig. 22. Relative maximum power current output of silicon solar cells after 720 hours of exposure at 80°C

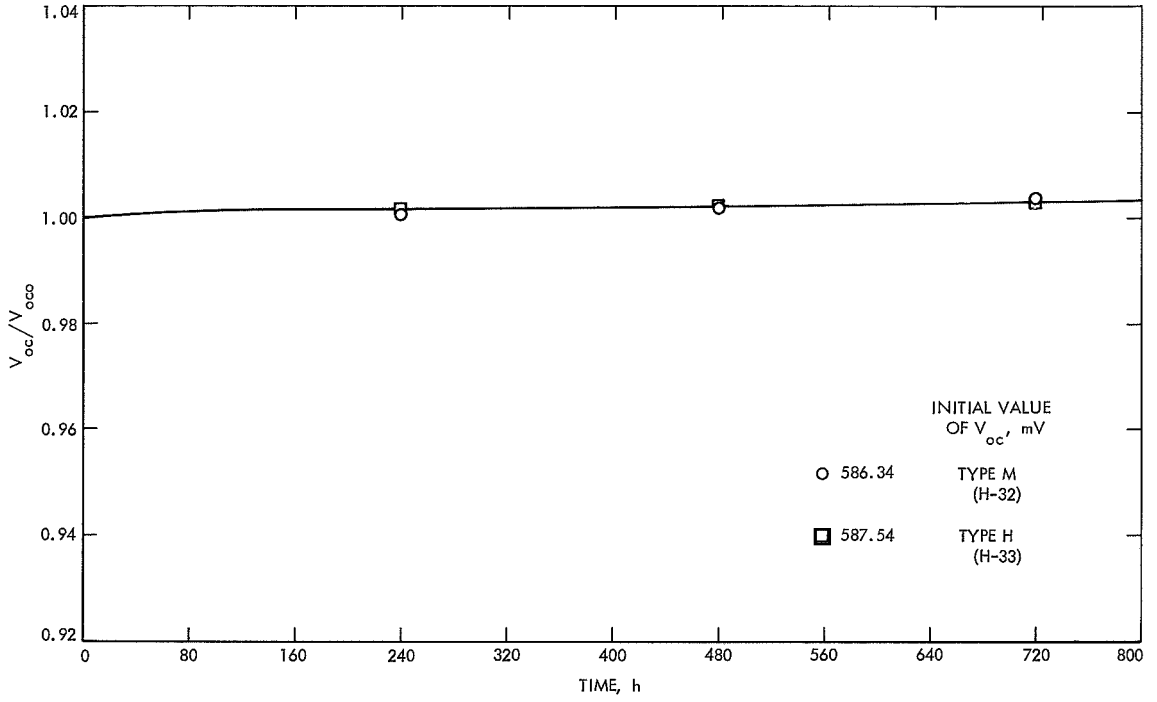

Fig. 23. Relative open-circuit voltage output of silicon solar cells after 720 hours of exposure at 80°C

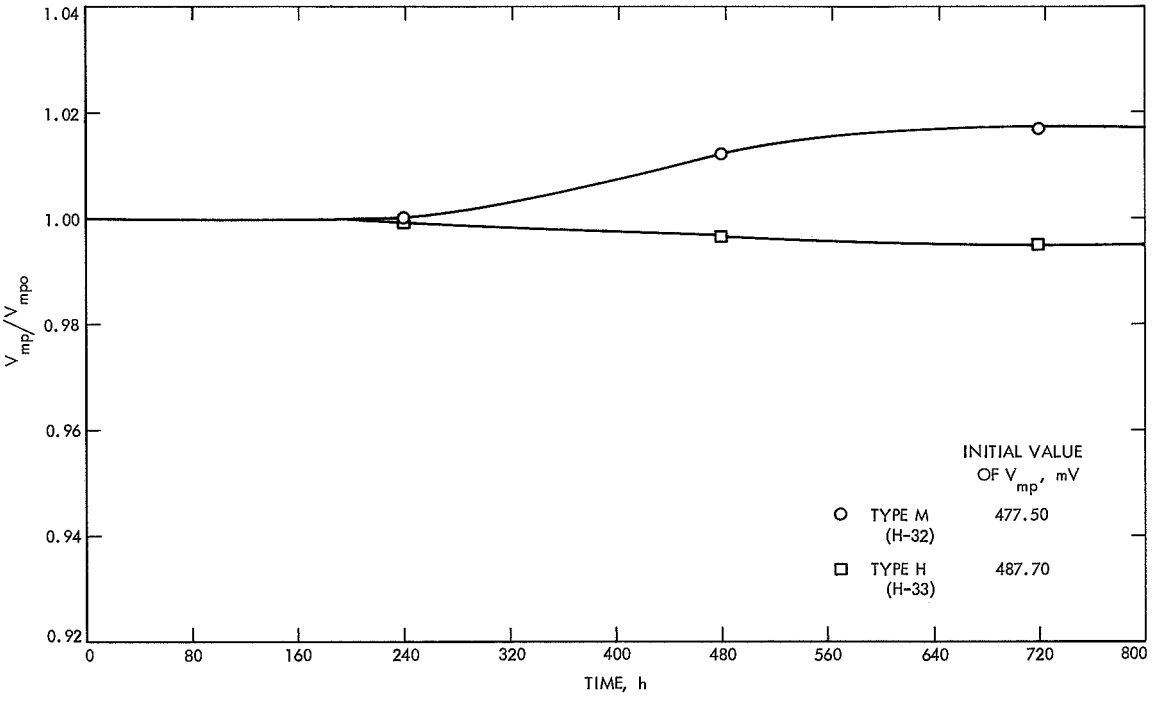

Fig. 24. Relative maximum power voltage output of silicon solar cells after 720 hours of exposure at 80°C

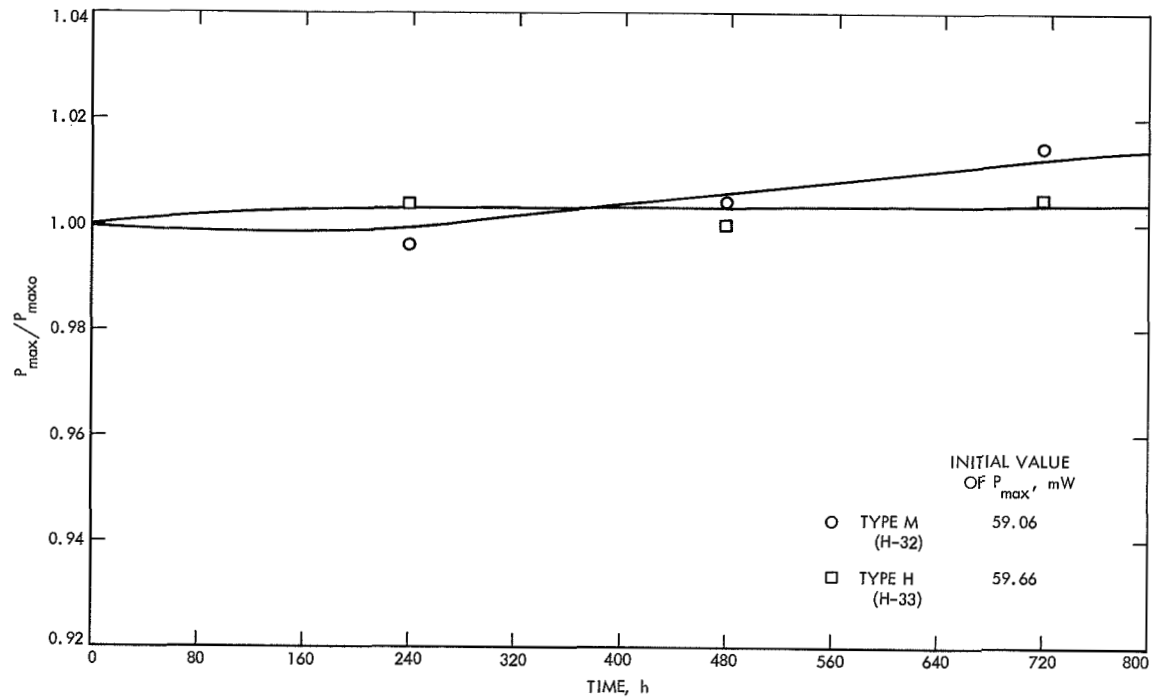

Fig. 25. Relative maximum power output of silicon solar cells after 720 hours of exposure at 80°C

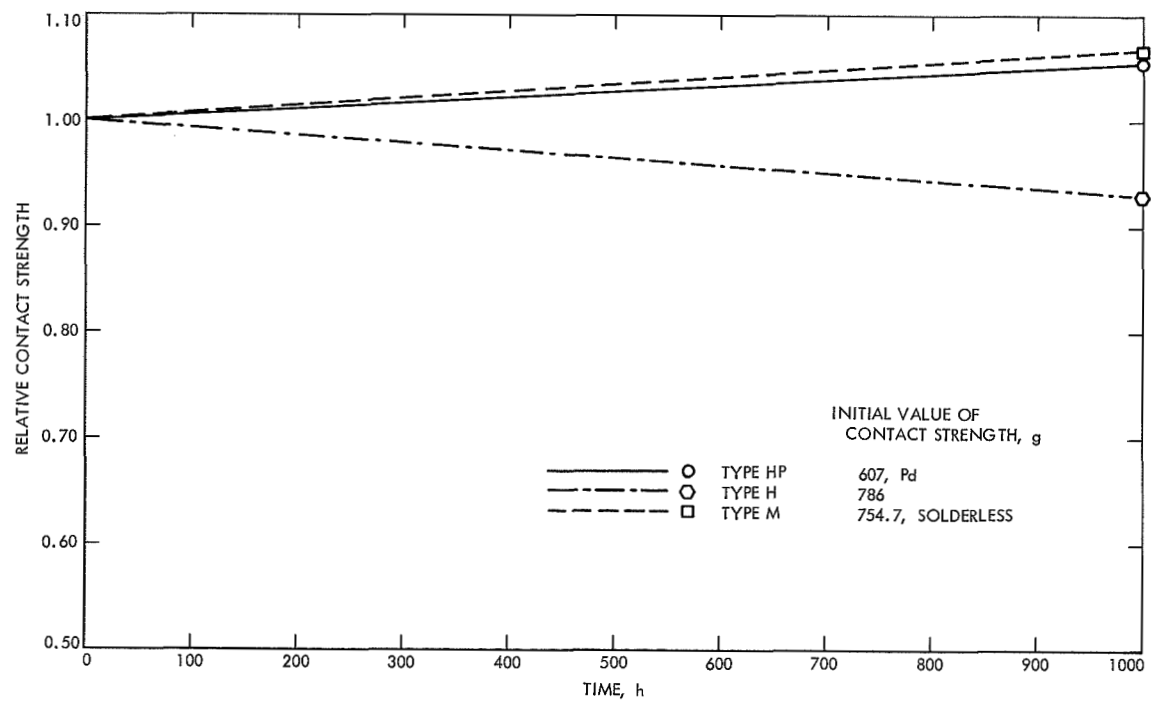

Fig. 26. Relative top contact strength of silicon solar cells after exposure to LN_2 at −196°C

increase of approximately 0.5% after 720 h, which is probably within measurement accuracy. In the high-humidity, high-temperature tests, the type M cells had exhibited a power decrease of about 11% and the type H cells a power decrease of about 36%. However, as discussed previously, much of the power degradation was attributed to degradation of the silicon monoxide antireflective coating, and it is difficult to determine which portion of the power degradation, if any, is attributable to contact degradation.

In the 150°C storage test the relative maximum power of the type H cells, as shown in Fig. 7, exhibited no change as a function of the environment, while the type M cell exhibited a power decrease of about 2% after 720 h. Thus the higher temperature of 150°C affected both the mechanical and electrical stability of the type M, silver–titanium solder-coated cell, while the lower temperature of 80°C did not. (This was not the case with the type H-11 silver–titanium solder-coated "corner-dart" contact cells, which exhibited neither electrical nor mechanical degradation at 150°C.)

D. Temperature Soak, −196°C (Liquid Nitrogen)

As shown in Table 1 three cell types were investigated at a storage temperature of −196°C, namely, type HP, palladium-containing silver–titanium solderless contact, type H, non-palladium-containing silver–titanium solderless contact, and type M, non-palladium-containing silver–titanium solder-coated contact. Since eight measurements were made (up to the cumulative exposure of 1000 h) the 1000-h cells were, in fact, subjected to eight thermal shock cycles, from room ambient to liquid nitrogen back to room ambient conditions, which were superimposed upon the soak itself. The types H and M cells were chosen for investigation since these are the most commonly used cell types for flight use, and the HP type cell was chosen to investigate the effects of palladium on the cell characteristics at liquid nitrogen storage temperatures.

1. Mechanical characteristics. The relative top contact strength of the three cell types is shown as a function of exposure time in Fig. 26. A slight increase of top contact strength of about 5% was found after 1000 h exposure time for the palladium-containing cell and the type M (silver–titanium solder-coated contact), while an approximate 7% decrease in contact strength was exhibited by the non-palladium-containing solderless contact cell type H. However, on an absolute basis the palladium-containing cell had the lowest postexposure contact strength because of its initially (unexposed) lower contact strength.

The relative bottom contact strength as a function of exposure time for the three cell types is shown in Fig. 27. These results contrast quite markedly with the top contact strengths shown in Fig. 26. The type H cell (non-palladium-containing, solderless silver–titanium) appears to be quite stable over the 1000-h test time. The palladium-containing silver–titanium type HP cell exhibited a degradation of greater than 10%, and the type M cell, solder-coated silver–titanium, exhibited a very dramatic decrease of more than 40% in back contact strength. This drastic difference of the behavior of the solder-coated cell is attributed to the mismatch in the thermal coefficient of expansion between solder and silicon, which causes considerable stressing at the liquid nitrogen temperature. The fact that the back contact lost a very great percentage of its initial strength for the M type cell, while the front contact appeared to be stable, is probably due to the fact that the back contact is an area contact which magnifies the stresses involved. It should be noted, however, that the absolute contact strengths of all three cell types at the end of 1000 h were quite similar to one another, since the type M cell initially had a much higher pull strength than the other two cell types. There is a significant possibility that the degradation of mechanical strength of the solder-coated type M cells would be even more severe when the cells are interconnected and bonded to a substrate. The solar cell user should certainly consider this possibility.

2. Electrical characteristics. The relative short-circuit current of the three cell types as a function of exposure time is shown in Fig. 28. All three cell types exhibited an initial (slight) increase in short-circuit current and then remained stable over the period of the test (1000 h). The relative maximum power current as a function of exposure time is shown in Fig. 29. All the cell types appear to be quite stable over 1000-h test time, the type H cell exhibiting an increase of about 2%. The relative open-circuit voltage of the three cell types as a function of exposure time is shown in Fig. 30 and indicates a high degree of stability for all three cell types. The relative maximum power voltage as a function of exposure time for the three types is shown in Fig. 31. While the curves appear to go through some interesting gyrations, the magnitude of the gyrations is not considered to be significant, and all three cell types appear to be quite stable. After 1000 h, cell types M and HP were approximately 0.5% higher and cell type H approximately 0.5% lower than the initial values.

The relative maximum power output of the three cell types as a function of exposure time is shown in Fig. 32.

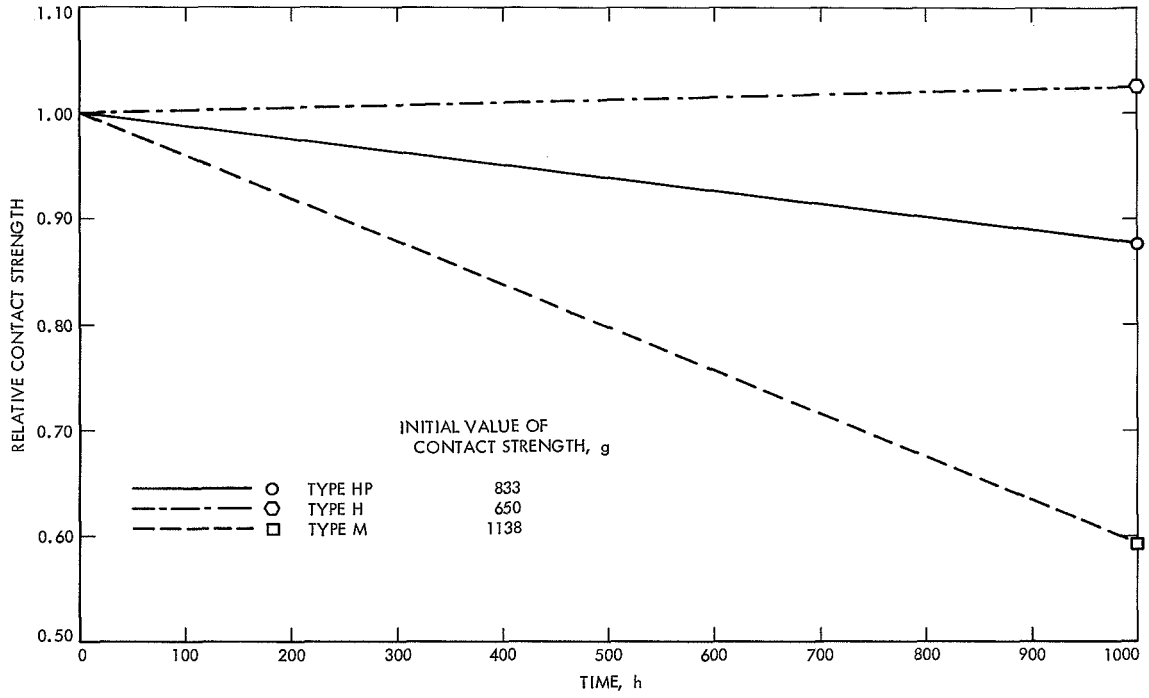

Fig. 27. Relative bottom contact strength of silicon solar cells after exposure to LN_2 at −196°C

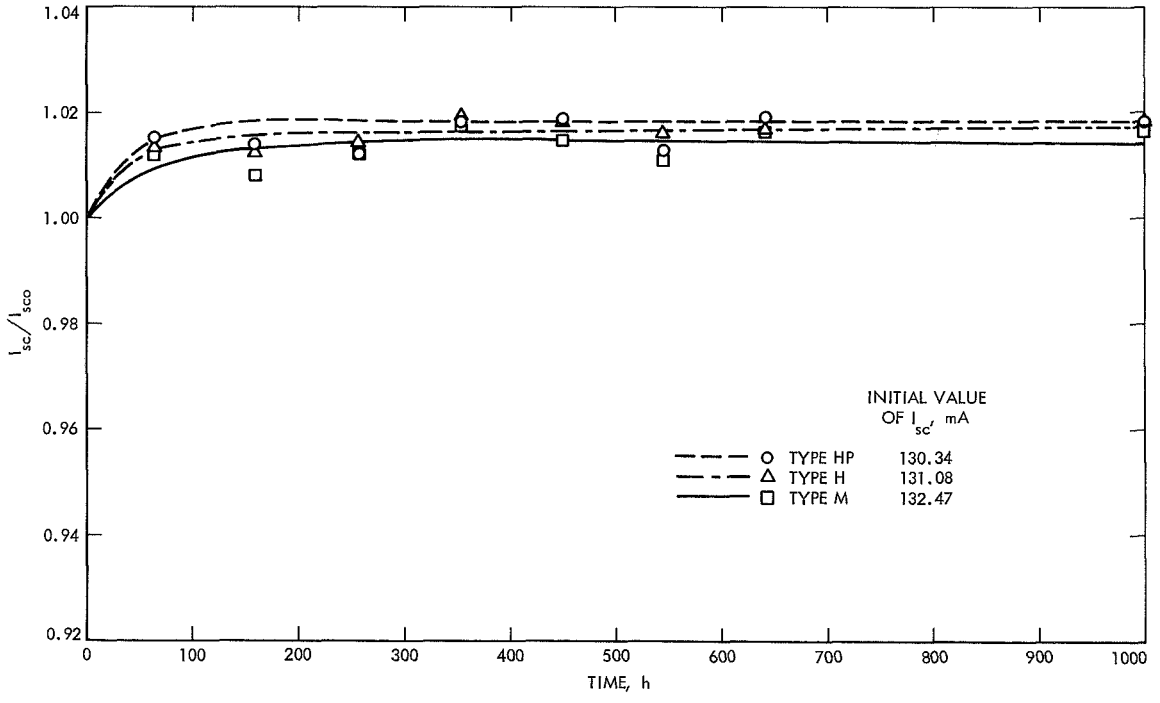

Fig. 28. Relative short-circuit current output of silicon solar cells as a function of time after exposure to LN_2 at −196°C

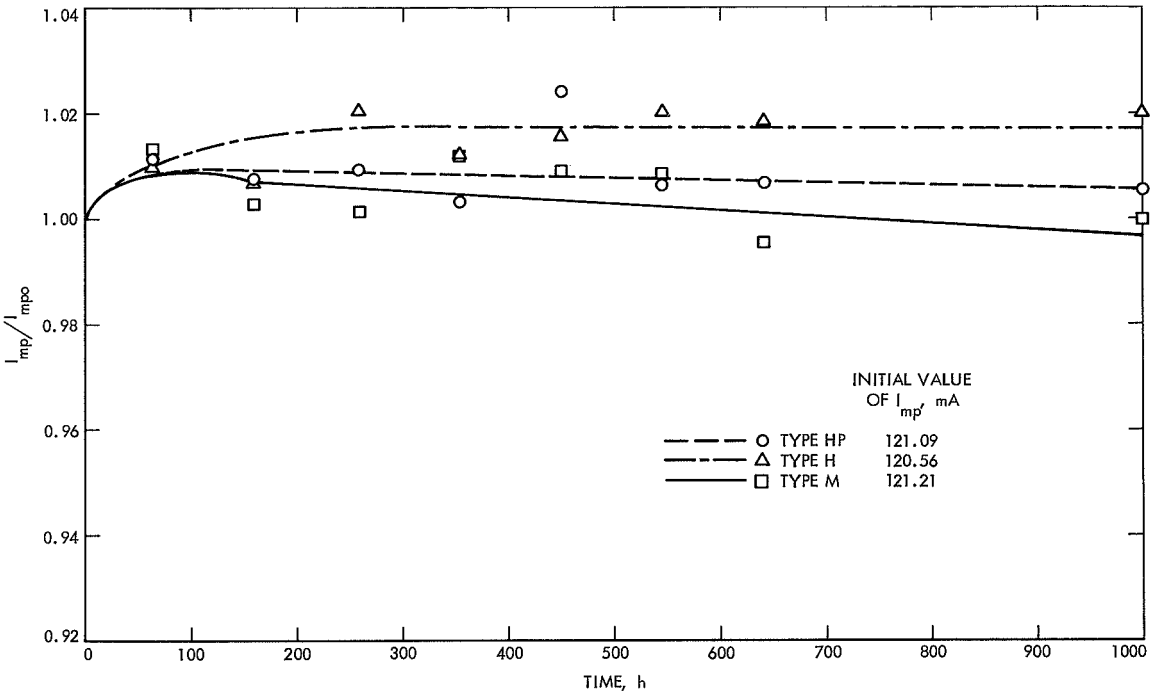

Fig. 29. Relative maximum power current output of silicon solar cells as a function of time after exposure to LN_2 at −196°C

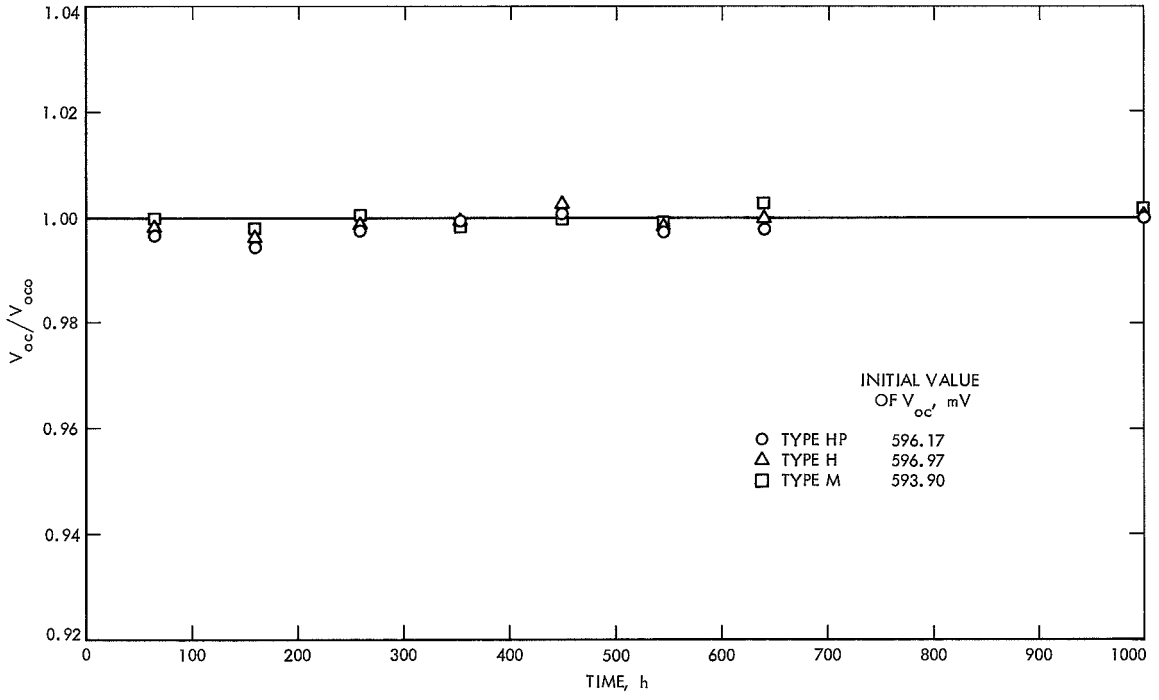

Fig. 30. Relative open-circuit voltage output of silicon solar cells as a function of time after exposure to LN_2 at −196°C

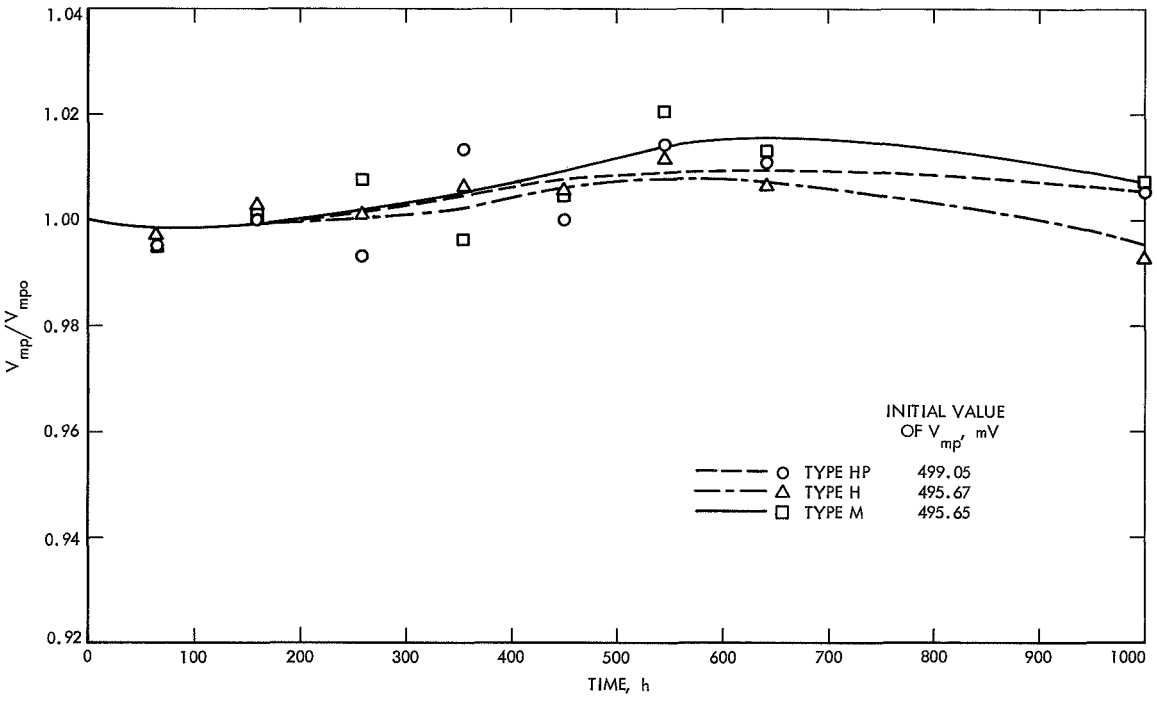

Fig. 31. Relative maximum power voltage output of silicon solar cells as a function of time after exposure to LN_2 at −196°C

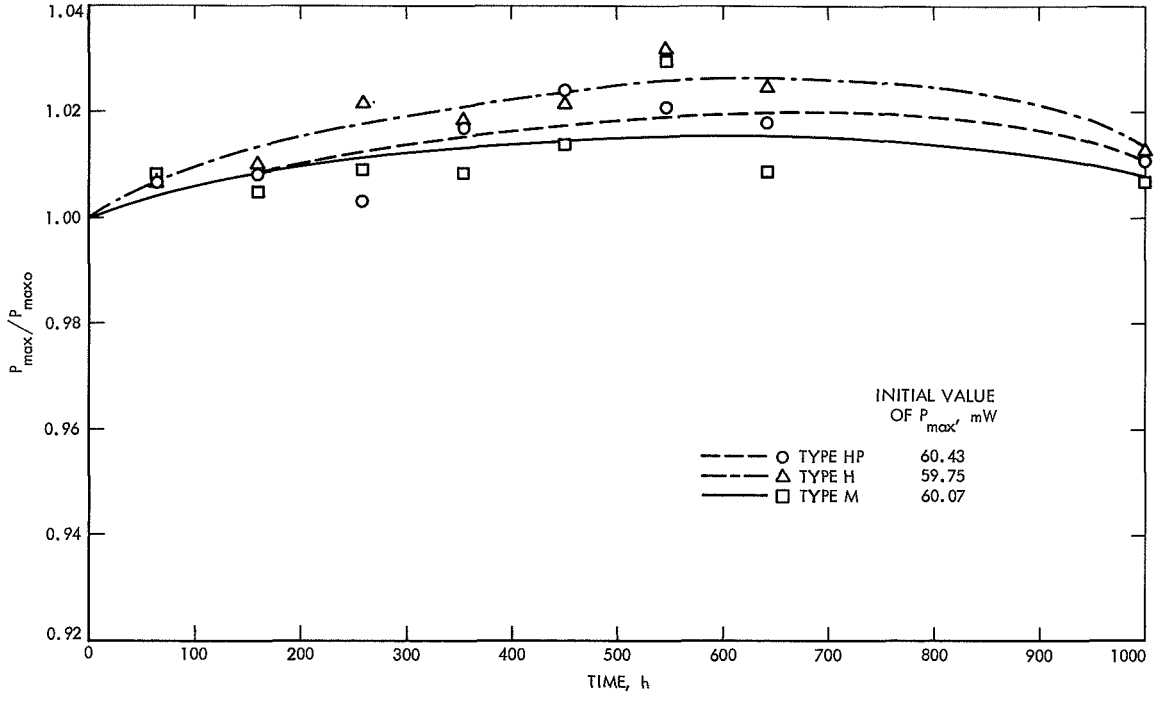

Fig. 32. Relative maximum power output of silicon solar cells as a function of time after exposure to LN_2 at −196°C

The three cell types appeared to increase in maximum power, peaking at an exposure time of about 550 h. Cell types H and M exhibited a power increase of about 3%, and type HP exhibited an increase of about 2%. After 1000 h, all three cell types exhibited an increase of about 1% in maximum power output. Thus the severe percentage contact degradation of the type M (solder-coated, silver–titanium contact) back surface contact strength does not appear to have adversely affected the electrical characteristics of this cell type as a result of storage at −196°C for periods up to 1000 h. This is in agreement with previous conclusions (Ref. 3) that electrical stability and mechanical stability cannot be inferred from one another. In general, the electrical characteristics of all three cell types, on an absolute as well as on a relative basis, appear to be quite similar, the differences being well within experimental error.

V. Conclusions

Some extremely interesting conclusions can be drawn from the series of tests described in this report, especially when correlated to the high-humidity, high-temperature test previously reported (Ref. 1). The results of the 80°C soak clearly show that the severe degradations observed in contact strength for the silver–titanium solderless cells were directly a result of the combined humidity/temperature environment and not due to the temperature component alone. Exposure to an 80° temperature for 720 h appears to be a very benign environment, resulting in no discernible degradation of either mechanical or electrical properties. When combined with a relative humidity of 95 percent, however, this environment can be extremely severe for contact systems without solder coating.

The MM69 submodule design, including choice of cell type, contact system, and interconnects, was clearly shown to be superior to that of the MV67 submodule design for exposure to 1000 h at 125°C.

Comparison between results of the 80 and 150°C soaks indicates that the solder-coated silver–titanium M-type cell is adversely affected as the temperature is increased, probably because of the interaction of the tin component of the solder and the silver at the 150°C temperature. In this case, for temperatures of 150°C, the absence of solder seems desirable. At liquid nitrogen temperatures, the solder coating also appears to adversely affect the mechanical stability of the back contact owing to the thermal expansion coefficient mismatch between solder and silicon, although on an absolute pull strength basis the solder-coated contact appeared to be no worse than the non-solder-coated contacts. The inherent solder–silicon thermal expansion coefficient mismatch might, however, be even more detrimental when the cells are interconnected and bonded to a substrate, and consideration should be given to this possibility. The addition of palladium to the solderless silver–titanium contact system appeared to present no advantages for the environments studied here.

The MM69 type cell, solder-coated silver–titanium contacts, appears to be as good if not better than other cell types in all environments studied so far (including high-humidity, high-temperature) except for exposures at temperatures of +150 and −196°C. For these cases, the MM69 type cell is inferior to the solderless cell contact system.

In the case of the +150°C exposure, it should be pointed out that although the solder-coated M-type cells exhibited mechanical and electrical degradation, the solder-coated H-11 type cells did not. The only difference between the contacts of the two cell types was one of configuration, not composition (both cell types had silver–titanium solder-coated contacts), the former cell type utilizing a "bar" contact and the latter cell type utilizing a "corner dart" contact on the active cell face. The configuration difference would not be expected to influence the mechanical strength of the back contacts, which were similar for the two cell types. The fact that the H-11 type cells did not exhibit the degradation in back contact strength, as was observed in the case of the M-type cells, indicates that the presence of solder need not *necessarily* result in degradation at 150°C exposure, but that such degradation is a possibility. Thus for some missions there may be a tradeoff between protection against humidity degradation of contacts and protection against detrimental effects of extremely high or low temperature on the cell contacts.

In general, the lithium-containing cells exhibited electrical and mechanical contact stability as good as, if not better than, the other cells tested at the +150°C exposure temperature.

Appendix

Solar Cell Submodules

The submodule consisting of solar cells connected in parallel is commonly used as the basic building block for construction of solar arrays. This report describes the effects of temperature storage on two basic cover-glassed submodule designs employed by JPL over the past years. The *Mariner* Mars 1969/71 submodules consist of *n–p* silicon solar cells having dimensions of 2 × 2 × 0.046 cm. The nominal base resistivity of these cells ranges from 1 to 3 ohm-cm; the cells have vacuum-deposited, titanium–silver solder-coated contacts. Earlier submodule designs employed on *Mariner* Venus 67 and *Surveyor* spacecrafts SC-5, 6, and 7 consisted of *p–n* cells with dimensions of 1 × 2 × 0.046 cm. The *p–n* cells had the same nominal base resistivity, but differed in the type of metallized contact system. The *p–n* cells had gold-flashed, electroless, nickel-plated solder-coated contacts.

The basic differences between the two types of submodules are shown in Fig. A-1. Both submodule designs use Kovar bus bar interconnections. Kovar is a metal alloy made up of iron–nickel and cobalt. This metal alloy was selected because its thermal coefficient of expansion is similar to that of silicon. The *n–p* submodule design used tin-plated ribbon interconnectors for both the top and bottom cell contacts. The *p–n* design used a gold-plated 0.051-cm-diam (0.020-in.) wire for the top contacts and a flat ribbon bus bar configuration for the bottom contacts. Both submodule designs were assembled in graphite soldering boats using tunnel oven soldering technique (Ref. 4).

The tunnel oven soldering machine was developed by Missimers for JPL to eliminate soldering variables that usually exist such as in the case of hand-soldering even under optimum processing conditions. The semiautomated tunnel oven process was developed to minimize thermal stress during soldering. The submodules were designed so that all soldering connections made directly to the cells could be performed before assembly of the submodules to the panel.

The *n–p* submodules utilized 0.051-cm (0.020 in.) 7940 fused silica cover glass, and the *p–n* submodules used 0.015-cm (0.006-in.) 0211 microsheet cover glasses. Both cover glass types utilized a 0.410-μm cut-on interference filter and antireflective coatings. A silicone adhesive, RTV-602, supplied by General Electric, was used as cell-cover glass adhesive in both cases. The main reason for the change in cover glass material and thickness between the *p–n* and *n–p* modules was to provide additional radiation protection for the more recent *Mariner* solar arrays.

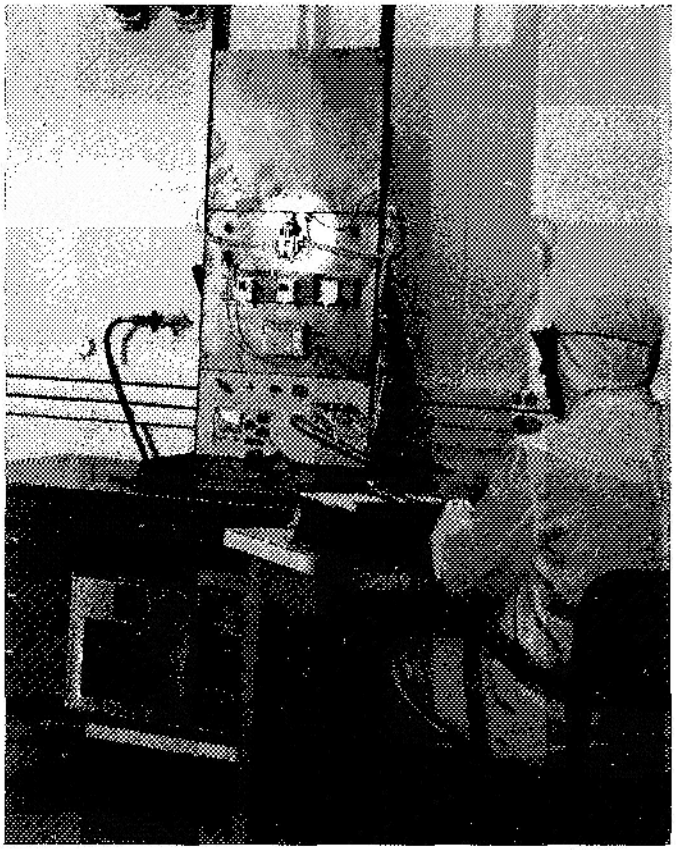

Fig. A-1. Electrical test facility

I. Contact Strength

One of the important areas of solar cell contact evaluation is that of pull or peel contact strength test. This test is accomplished by applying a load to a specified test tab which is bent perpendicular to the cell so that the applied load tends to peel the soldered tab off the cell. Acceptable values of this pull or peel strength are established for specific bus bar designs by empirical tests. However, this practice leaves two areas of uncertainty, namely, (1) there is no way at present to correlate the magnitude of the tab loading with respect to the actual stress field in the cell, and (2) there is no way to extrapolate acceptable tab load values from one interconnector design concept to another.

Consequently, studies (Ref. 5) have been under way at JPL to perform a detailed analysis of the stress distribution of the tab-to-cell interface under loading conditions of the pull or peel test. Since test data for most cells have been obtained over a wide temperature range (−180 to +180°C), correlations can be made between analytical and empirical results. This analysis could then be extended to other designs, modifications of current designs, and effects of degrading environments. To provide a comparison between cell and module contact strengths prior to any environmental exposure, pull tests were conducted on unexposed *n–p* and *p–n* cells and modules representative of those considered in this report. The results of these tests are shown in Table A-1 and indicate that, in general, the contact strengths as measured on the cells can be about 25% higher than those measured on actual modules using the interconnectors as the pulling member. This appears to be the case for both wire-type and ribbon-type interconnectors.

Table A-1. Comparison between cell and module contact pull strength (Room temperature ambient conditions)

Type	Top contact strength, g		Cell bottom contact strength, g
	Cell (avg of 10)	Module (avg of 6)	
MM69/71 (*n–p* Cells)	1816	1430[a]	1557
MM67/Surveyor (*p–n* Cells)	1549	1150[b]	1274

[a]Ribbon-type interconnector.
[b]Wire-type interconnector.

II. Test Facility

The test facility used to determine the cell electrical characteristics is shown in Fig. A-1. The light source is an X25L solar simulator. The oven used for the 125 and 150°C temperature soaks is shown in Fig. A-2. The cells were loaded on an aluminum tray with the active cell surface upward. The oven used for the 80°C temperature soak is shown in Fig. A-3. Again, the cells were loaded, active face upward, on an aluminum tray. The test setup for the liquid nitrogen (−196°C) soak is shown in Fig. A-4. The cells were separated in a teflon-coated cage and manually immersed in a dewar flask containing the liquid nitrogen.

Fig. A-2. High-temperature oven (125—150°C soaks)

The pulse-resistance soldering machine used to attach the contact strength test tab to the cell contacts is shown in Fig. A-5. A photograph showing a typical solar cell mounted in the contact strength pull test machine is shown in Fig. A-6. A comparison between contact strength tests on conventional *n–p* cells and lithium-doped *p–n* cells is shown in Fig. A-7. Cracking of the cell as shown in Fig. A-7b was a common failure mode for the *p–n* lithium-doped cell. Figure A-8 is a photograph of the contact pull strength test machine, the environmental chambers, and associated monitoring and recording equipment.

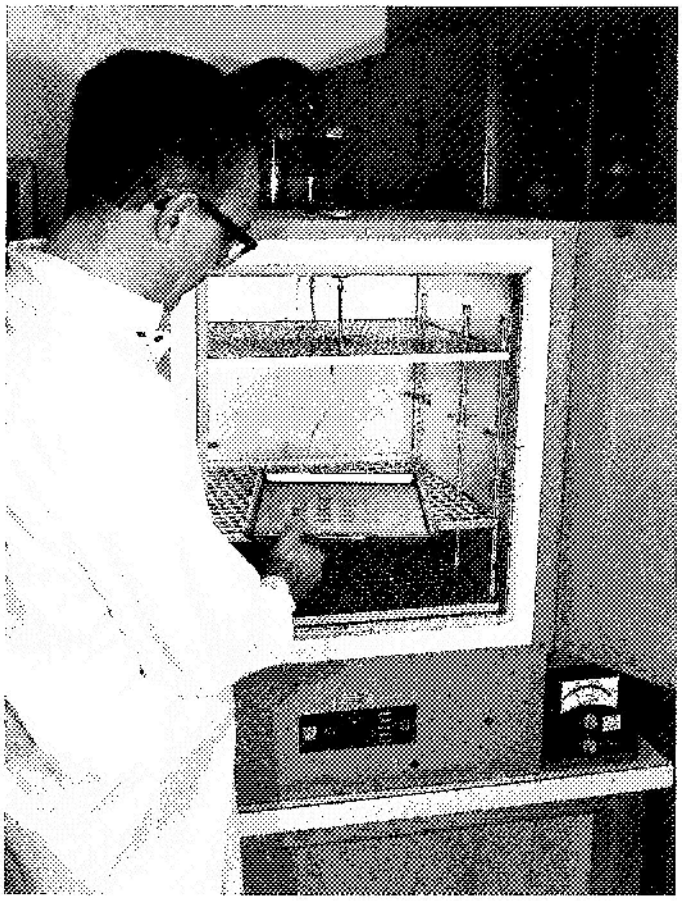

Fig. A-3. Temperature oven (80°C soak)

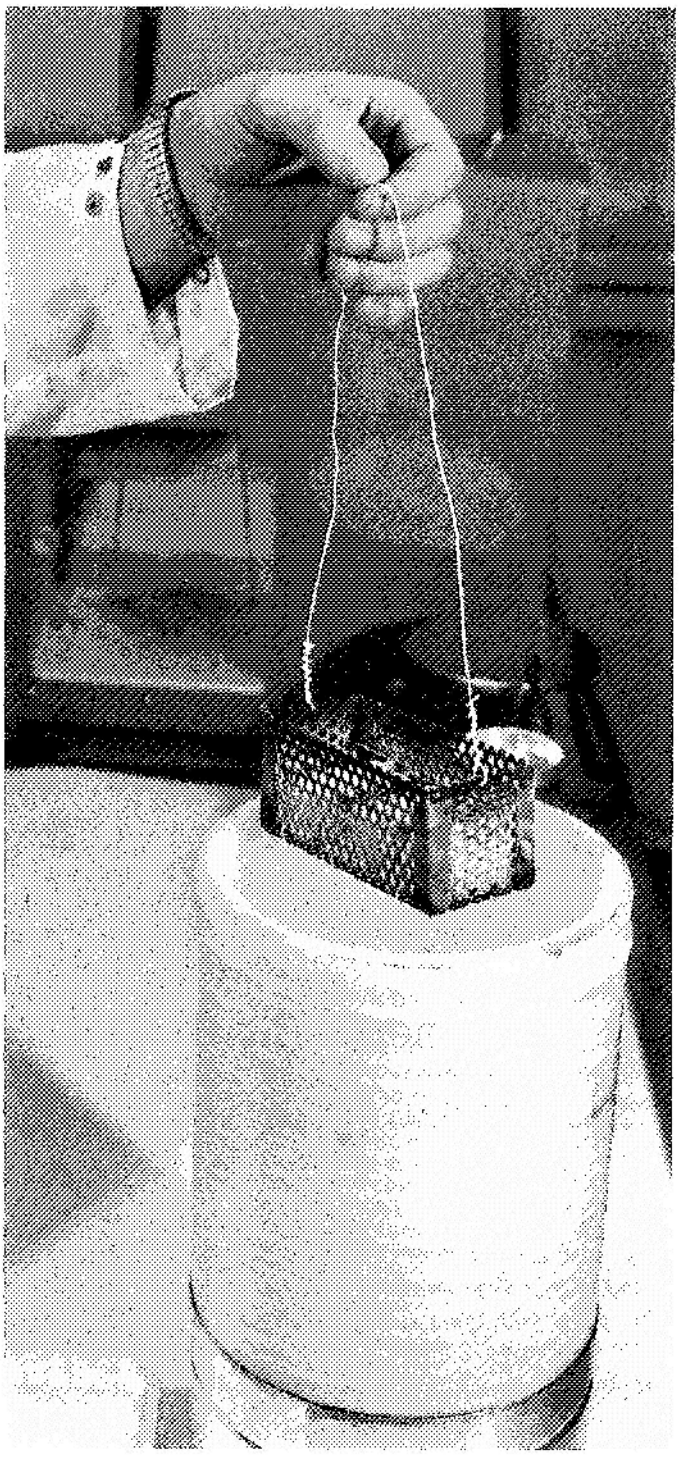

Fig. A-4. Low-temperature storage (−196°C)

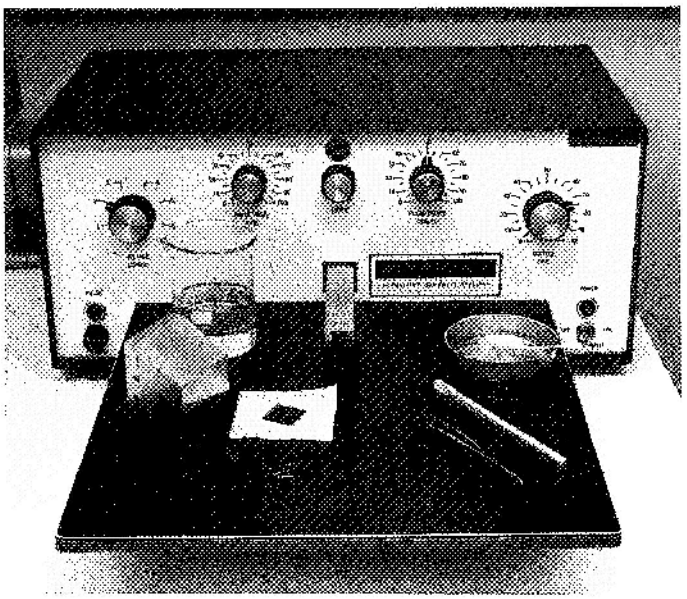

Fig. A-5. Pulse resistance soldering machine

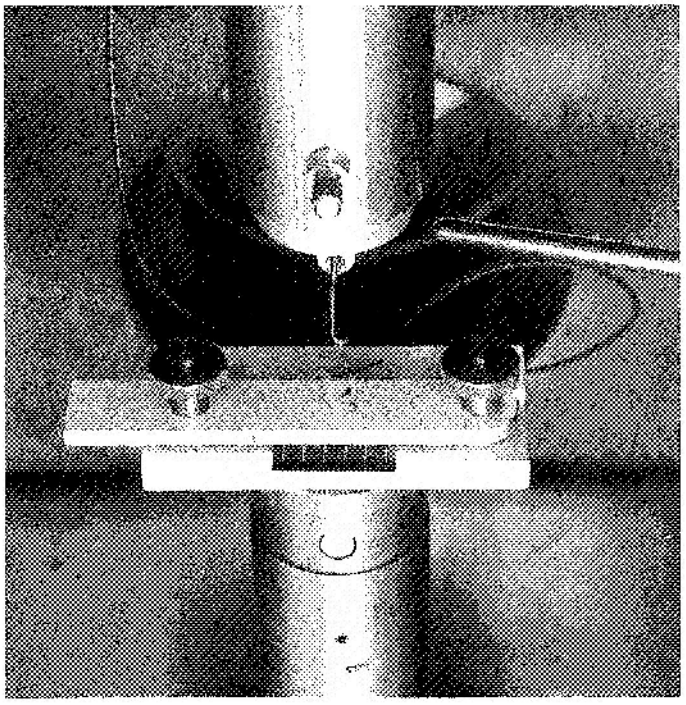

Fig. A-6. Solar cell mounted in contact strength test machine

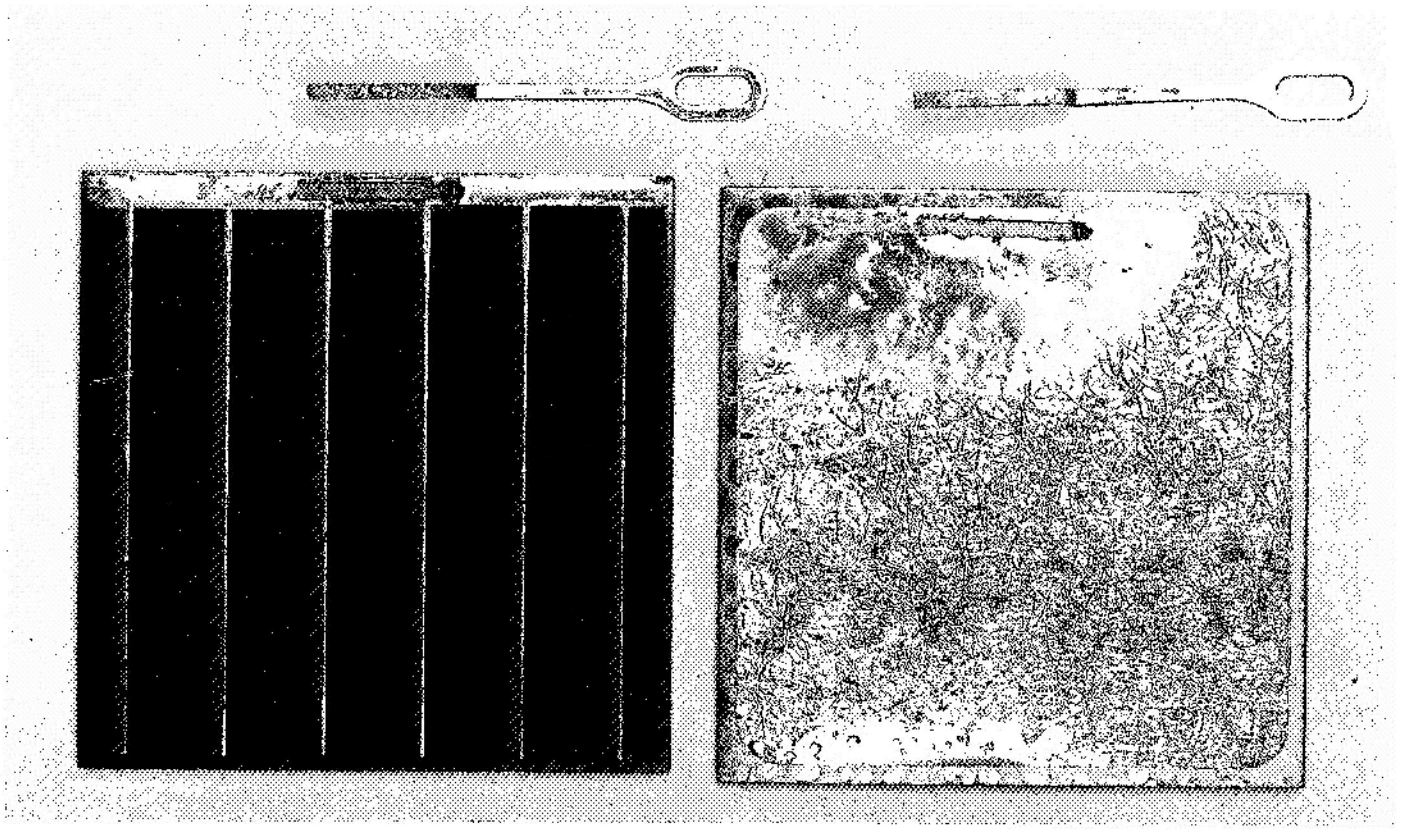

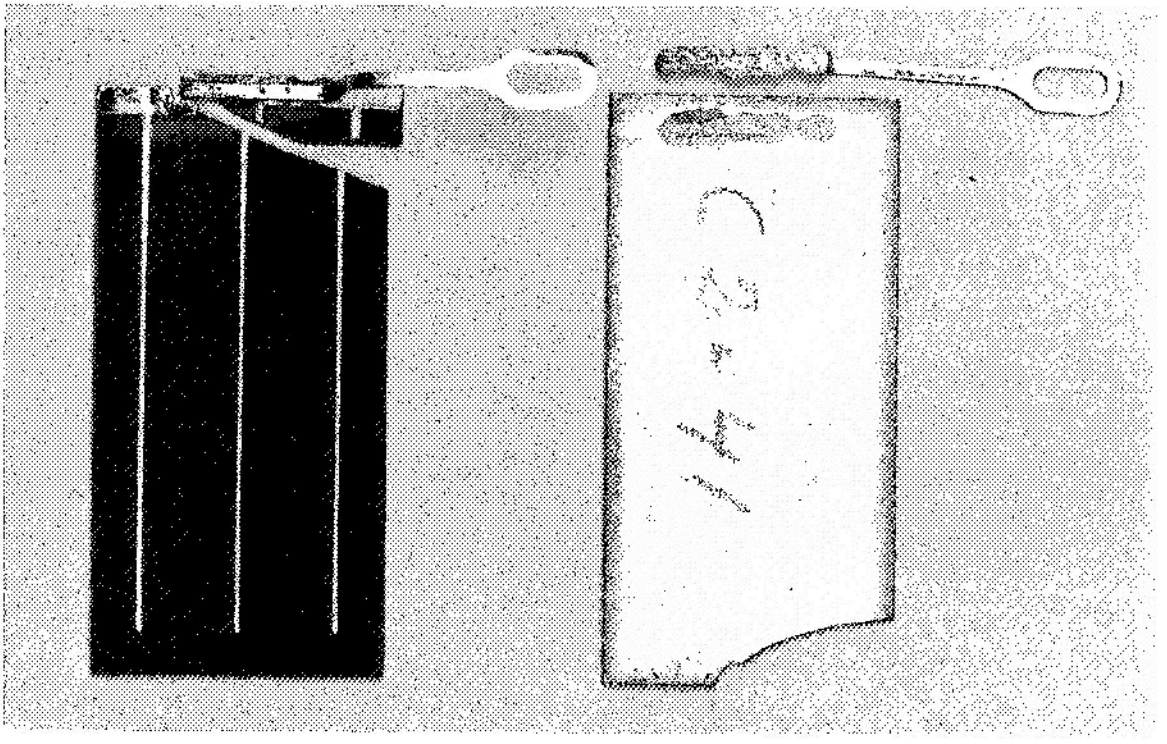

Fig. A-7. Comparison between results of pull strength test on (a) *n–p* cell and (b) lithium-doped *n–p* cell

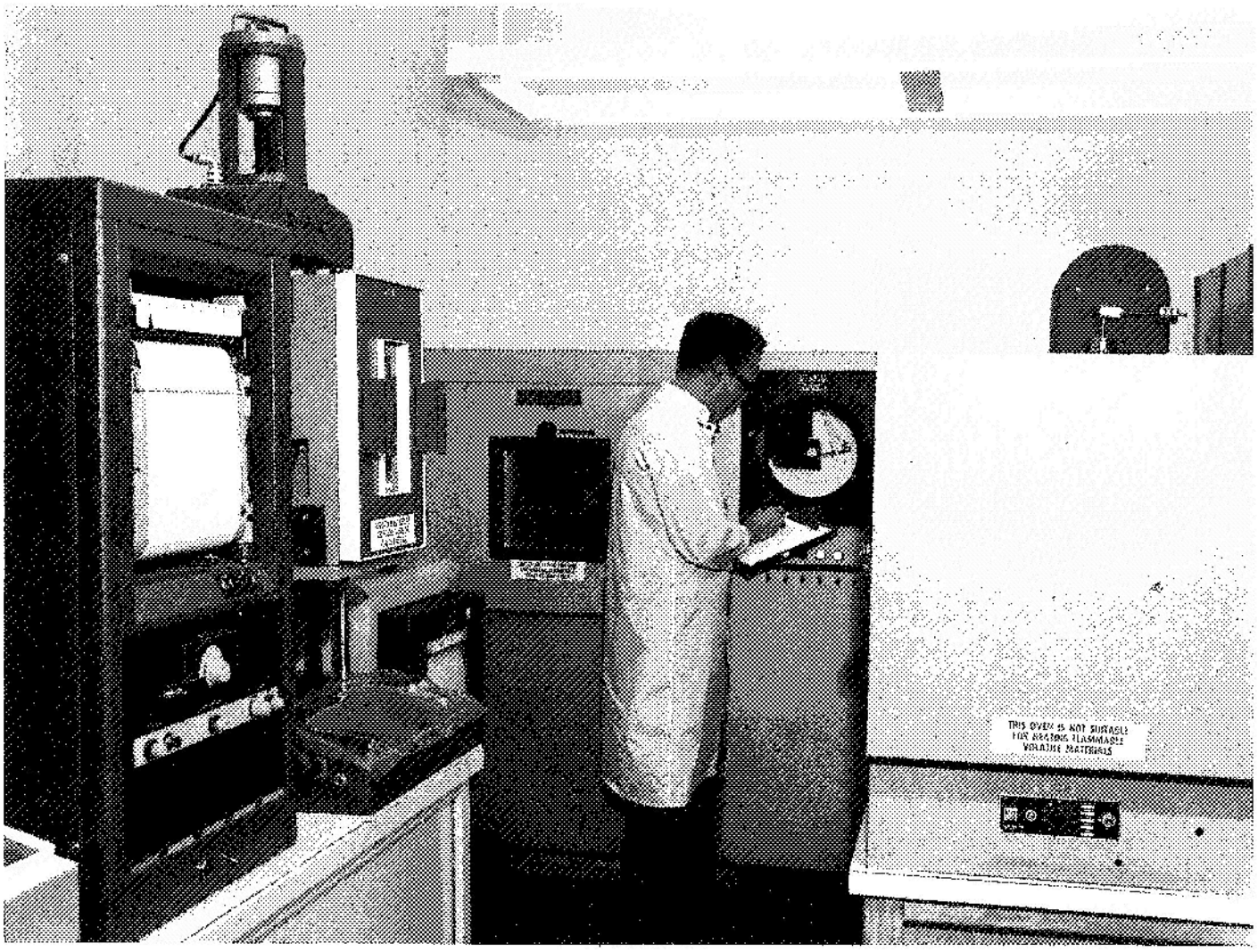

Fig. A-8. View of Instron testing machine, environmental chambers, and associated recording equipment

References

1. Yasui, R. K., and Berman, P. A., *Effects of High-Temperature, High Humidity Environment on Silicon Solar Cell Contacts*, Technical Report 32-1520. Jet Propulsion Laboratory, Pasadena, Calif., Feb. 1971.

2. Berman, P. A., and Yasui, R. K., *Data Support Package: Effects of Storage Temperatures on Silicon Solar Cell Contacts*, JPL Technical Memorandum 33-497. Jet Propulsion Laboratory, Pasadena, Calif., Oct. 15, 1971.

3. Moss, R., and Berman, P., *Effects of Environmental Exposures on Silicon Solar Cells*, Technical Report 32-1362. Jet Propulsion Laboratory, Pasadena, Calif., Jan. 15, 1969.

4. Yasui, R. K., "Solar Cell Submodule Design and Assembly," in Conference Record of the Intersociety Energy Conversion Engineering Conference, held in Miami, Florida, Aug. 1967.

5. Butterworth, L. W., and Yasui, R. K., *Structural Analysis of Solar Arrays*, Technical Report 32-1528. Jet Propulsion Laboratory, Pasadena, Calif., May 15, 1971.

NASA — JPL — Coml., L.A., Calif.

~~06642~~ N71-37622

TECHNICAL REPORT STANDARD TITLE PAGE

1. Report No. 32-1541	2. Government Accession No.	3. Recipient's Catalog No.
4. Title and Subtitle EFFECTS OF STORAGE TEMPERATURES ON SILICON SOLAR CELL CONTACTS		5. Report Date October 15, 1971 6. Performing Organization Code
7. Author(s) Paul Berman, R. K. Yasui		8. Performing Organization Report No.
9. Performing Organization Name and Address JET PROPULSION LABORATORY California Institute of Technology 4800 Oak Grove Drive Pasadena, California 91103		10. Work Unit No. 11. Contract or Grant No. NAS 7-100 13. Type of Report and Period Covered Technical Report
12. Sponsoring Agency Name and Address NATIONAL AERONAUTICS AND SPACE ADMINISTRATION Washington, D.C. 20546		14. Sponsoring Agency Code

15. Supplementary Notes

16. Abstract

Solar cells having various contact systems and configurations were investigated to determine the effect of storage temperature and duration on cell electrical and mechanical characteristics. Cells having n diffused into p-base silicon, p diffused into n-base silicon, and p diffused into n-base lithium-containing silicon were studied. Contact systems of silver-titanium, silver-titanium with solder coating, silver-titanium with palladium, and electroless nickel were investigated. Also included in the study were submodules similar to those used in past JPL flight programs.

The results showed that electrical and mechanical degradations previously observed in high-humidity, high-temperature environment were the result of the combined environment and not due to the temperature component alone. Solder-coated silver-titanium contacts can be adversely affected by prolonged exposure to 150°C temperature soak and to -196°C liquid nitrogen exposure. The lithium-containing cells exhibited good electrical and mechanical contact stability with respect to the other cells tested at 150°C. The addition of palladium to the silver-titanium system presented no apparent advantage for the 150°C temperature soak, except in the case of relative top contact strength, where stability (but not absolute pull strength) was superior to the other cell types.

17. Key Words (Selected by Author(s))	18. Distribution Statement
Electronic Components and Circuits Materials, Nonmetallic Power Sources Solid-State Physics	Unclassified -- Unlimited

19. Security Classif. (of this report)	20. Security Classif. (of this page)	21. No. of Pages	22. Price
Unclassified	Unclassified	34	